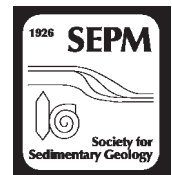


Journal of Sedimentary Research

Journal of Sedimentary Research, 2007, v. 77, 1003–1025
Research Article
DOI: 10.2110/jsr.2007.095



DIAGENESIS, POROSITY EVOLUTION, AND PETROLEUM EMPLACEMENT IN TIGHT GAS RESERVOIRS, TARANAKI BASIN, NEW ZEALAND

KAREN E. HIGGS,¹ HORST ZWINGMANN,² AGNES G. REYES,¹ AND ROB H. FUNNELL¹

¹GNS Science, 1 Fairway Drive, Avalon, P.O. Box 30-368, Lower Hutt, New Zealand

²CSIRO Petroleum, P.O. Box 1130, Perth, Western Australia 6102, Australia

e-mail: k.higgs@gns.cri.nz

ABSTRACT: Tight gas reservoirs have become popular targets in petroleum exploration in recent years, due largely to the increasing market demand for gas and also to technology advances used in extraction. Reservoir quality is typically poor due to deep-burial diagenesis, resulting in significant compaction, cementation, and illitization. However, analysis of tight reservoirs using integrated techniques can improve our understanding about the controls on reservoir quality, and these results can potentially be used to help predict reservoir quality at other sites.

The use of integrated analysis of diagenetic and burial history is here shown for the Eocene, K3E Kapuni Group reservoir in Cardiff-1, Taranaki Basin, New Zealand. The K3E belongs to a deep gas play that was considered uncommercial in the early 1990's due to poor reservoir quality associated with extensive authigenic illite. Potassium-argon dating has shown that destruction of the reservoir through illitization occurred in the Pliocene, associated with a late-stage heating and/or fluid-flow event.

Timing of illite authigenesis in the K3E reservoir postdates the likely circulation of CO₂-rich fluids that caused reaction of feldspar to form kaolinite and quartz. Homogenization temperatures from two-phase aqueous fluid inclusions within quartz cements, together with 1D basin models of CO₂ expulsion from coaly source rocks, indicate that feldspar reactions may have started in the mid Miocene. The CO₂-rich fluids are thought to have been generated by thermal decarboxylation of intraformational Paleocene–Eocene coals. At the same time, oil was being expelled from older, Cretaceous coals and migrated into the mid-late Eocene reservoirs; evidence for oil migration is demonstrated by the presence of residual oil and by the local occurrence of abundant oil-bearing fluid inclusions. The products of feldspar dissolution appear to be in reasonable balance with the amount of dissolved feldspar, suggesting a relatively “closed” diagenetic system with little improvement in reservoir quality despite the large volume of feldspar dissolved.

Petrographic evidence of reservoir sandstones at Cardiff-1 demonstrates the presence of some illite-free secondary macropores lined by residual oil. This local preservation of porosity may be replicating the original distribution of oil-saturated pores in the Pliocene, at the time when authigenic kaolinite underwent reaction to form illite. Remobilization of the oil probably occurred by gas flushing after the main phase of illitization at c. 5 Ma.

The data presented in this study are consistent with redistributed liquid petroleum into up-dip traps and represent the potential for a new exploration play. The Eocene reservoir at Cardiff-1 is currently gas-charged, with the pore system composed of approximately one third large macropores connected by a tortuous, microporous network. However, it is possible that, with the currently buoyant gas market and modern hydraulic fracturing techniques, it may now be economic to flow gas from the locally large pores identified in the K3E reservoir.

INTRODUCTION

Tight gas plays have received considerable attention in the past few years due to the strong gas market, reopening possibilities for previously uncommercial gas accumulations. The Cardiff structure, onshore Taranaki, New Zealand, is one such play and forms the focus for this study.

Cardiff-1 was drilled by Shell Todd Oil Services (STOS) in February 1992 to test two primary objectives in the mid-late Eocene Kapuni Group (K1A sandstone and K3E sandstone). Total depth of the well was at 5065 m along-hole below derrick floor (AHBDF; 4758 m true vertical subsea depth) at the base of the stratigraphically lower objective (K3E).

Very slow drilling rates were encountered through the K3E sandstone because of the extremely hard formation, resulting in severe hole caving.

Gas and condensate was encountered in both of the objectives. The main hydrocarbon-bearing interval is within the upper part of the K3E at 4738–4882 m AHBDF with an average water saturation (Sw) of 45% (STOS 1992). Approximately 29 m of net pay was also interpreted in the shallower K1A interval (4133–4172 m AHBDF) with an average Sw of 47% (STOS 1992). Despite good prognosis of sand presence from nearby wells, gas peaks reported during drilling (from mudlog with C₁–C₄ components commonly being present) and hydrocarbon accumulations interpreted from petrophysics, the Cardiff-1 well was plugged and abandoned. Both the K3E and K1A sandstones are interpreted to have

failed to produce commercial quantities of gas because of poor reservoir quality (STOS 1992).

Petrographic studies commissioned by STOS show that the sandstones have been considerably altered diagenetically and that the presence of common, widespread authigenic illite has severely restricted the permeabilities (Geotechnical Services 1992). In this study, samples from the K3E sandstone have been examined to explore controls on low permeability and to relate the diagenetic reactions to the history of burial and temperature and to the timing of oil expulsion from nearby kitchens. This integrated approach demonstrates the tools necessary to understand diagenetic and fluid-flow histories with implications for both exploration and reservoir management of deep gas plays. Conventional cores were not cut through the K1A sandstone at Cardiff-1, and therefore this shallower interval has not been included in the study.

Geological Setting

The Taranaki Basin is located along the west coast of New Zealand's North Island and is the main focus of oil and gas exploration in the country (Fig. 1). The basin is broadly divided into two structural regions, the Western Stable Platform and the Eastern Mobile Belt. The Western Stable Platform has remained relatively quiescent since the Cretaceous, and is characterized by "layer-cake" and progradational deposition on an unfaulted, subhorizontal and regionally subsiding sea floor (King and Thrasher 1996). By contrast, the Eastern Mobile Belt displays a complex morphology that is the product of tectonism associated with Neogene development of the Pacific-Austral convergent plate boundary through New Zealand.

At the broadest level, the Cretaceous-Cenozoic sedimentary record in the Taranaki Basin can be considered one major depositional cycle composed of four "megasequences" (Table 1; King and Thrasher 1996). Basin evolution began with late Cretaceous extensional faulting (syn-rift deposits) associated with the breakup of Gondwana and the formation of the Tasman Sea. The overlying Paleocene and Eocene deposits constitute a late-rift and post-rift transgressive sequence. They comprise the entirely marine Moa Group, which consists mainly of shelf and slope mudstones (Turi Formation), and the predominantly terrestrial and marginal marine Kapuni Group (Farewell, Kaimiro, Mangahewa, and McKee formations). Transgressive phases culminated in the early Miocene, and a regressive phase occurred from the mid-Miocene (Wai-iti and Ngatoro groups) to the present day.

The bulk of proven petroleum reserves in Taranaki are contained within the NE-SW trending fairway of the Kapuni Group (late-rift and post-rift sequence). These deposits were the primary objective for the Cardiff-1 well, located on a faulted four-way dip closure at the northern end of the Manaia Anticline trend, onshore Taranaki (Fig. 1). The Manaia Anticline was originally a graben depocenter for fluvial and shallow marine sedimentation during the Cretaceous-Eocene. The anticlinal structure developed in the earliest Miocene, at a time when the Manaia Fault Zone was established as a thrust-fault zone to the west, and the Tarata Thrust Zone was emplaced to the east.

Reservoir Description

The K3E sandstones form the main gas-condensate reservoir of the Kapuni Field, onshore Taranaki, where they have been interpreted by Bryant and Bartlett (1991) to represent a fluvial to estuarine sequence (Fig. 2). Stratigraphically, the MH2/MH1 miospore stage boundary is within the K3 interval, placing the K3E reservoirs at the base of the Mangahewa Formation (Fig. 2). In the onshore Taranaki region this formation encompasses coastal-plain through to shallow marine environments (King and Thrasher 1996).

At Cardiff-1 the Mangahewa Formation comprises approximately 960 m of section. The upper part is very heterolithic, composed of

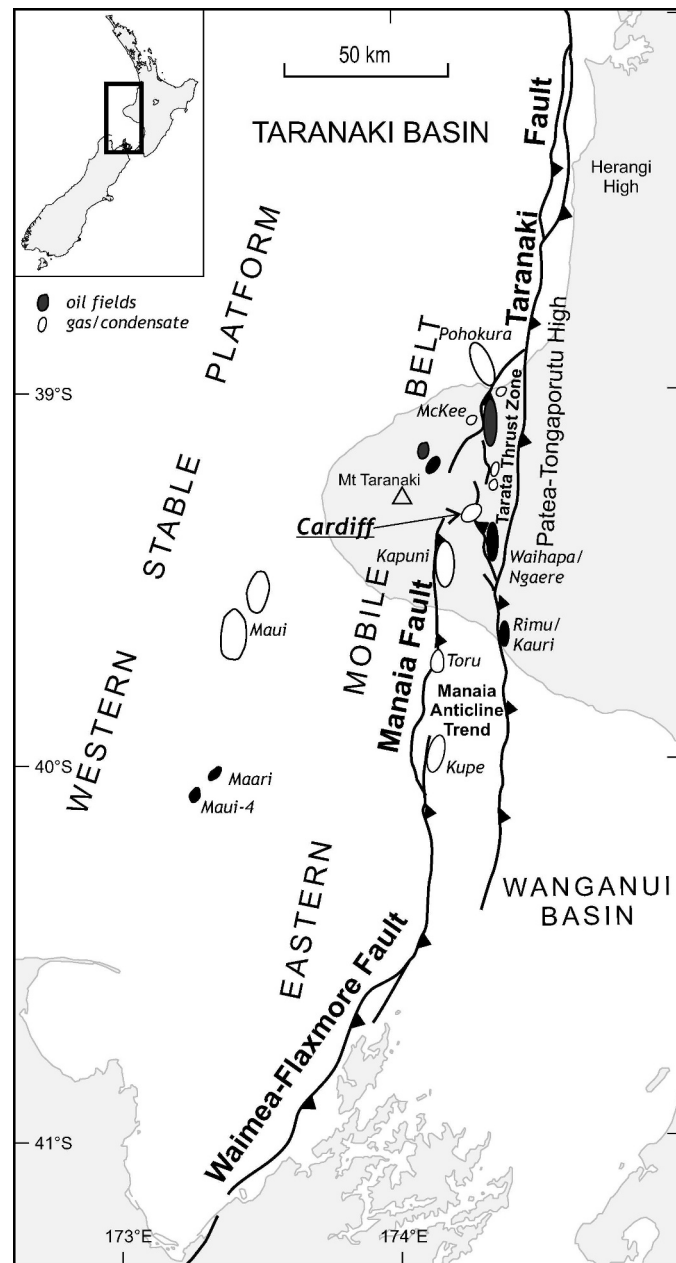


FIG. 1.—Location map for Cardiff structure, Taranaki Basin, New Zealand.

interbedded thin sandstone with siltstone, carbonaceous mudstone, and coal; these Mangahewa coals are a source for both oil and gas in the deep kitchen areas of the Taranaki Basin (e.g., Sykes 2001). The main reservoir sandstone at Cardiff-1 (K3E) underlies the thick coal-rich sequence and is composed of stacked sandstones. It can be subdivided into an upper and lower unit (K3EU and K3EL), where the upper K3E unit (K3EU) is marine-influenced and sand-dominated with a high net to gross (STOS 1992). In contrast to the Kapuni Field, the lower K3E unit (K3EL) at Cardiff-1 displays a relatively low net to gross composed of sandstone and siltstone interbedded with thin coals; these deposits are therefore interpreted as coastal-plain deposits and represent a slightly more proximal environment compared to the estuarine KE3L interpreted by Bryant and Bartlett (1991) for the Kapuni Field (Fig. 2).

TABLE 1.—Primary subdivision of the Cretaceous–Cenozoic succession in the Taranaki Basin (from King and Thrasher 1996).

Depositional Phase	“Megasequence”	Group	Basal Seismic Reflector
Regressive	4	Rotokare	Top Miocene
Transgressive	3 2 (late-rift and post-rift) 1 (synrift)	Wai-iti & Ngatoro Kapuni & Moa Pakawau	Top Eocene Top Cretaceous Top Basement

A 19 m core (core 2, 4780–4798.9 m MD) was taken through the upper KE3 reservoir unit at Cardiff-1 and reveals light gray, quartzose, noncalcareous to weakly calcareous, fine- to medium-grained sandstones with weak to moderate trough cross bedding (Fig. 3). Stacked sandstone beds are interbedded with more heterolithic intervals composed of mudstone and fine- to medium-grained sandstone. Burrows are moderately common in these beds and include *Ophiomorpha*, *Planolites*, and *Conichnus*. These observations are consistent with the marine-influenced environment interpreted by STOS (1992).

Conventional core analysis data from the cored interval illustrate the tight nature of the K3E reservoir at Cardiff-1, with maximum permeability values of 3.3 mD and 1.9 mD (horizontal and vertical

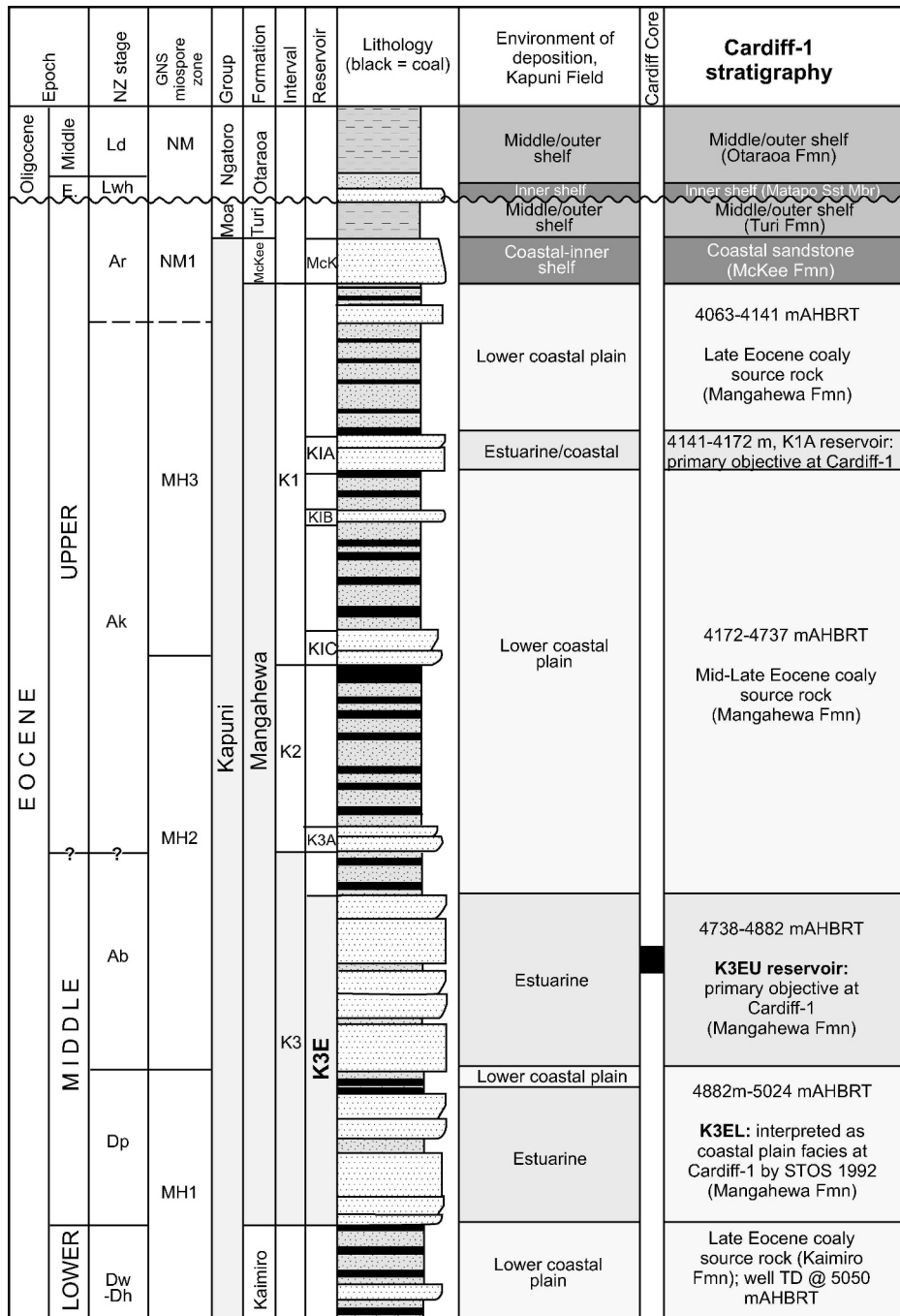


FIG. 2.—Representative Kapuni Group stratigraphy developed for the Kapuni Field and applied to stratigraphy at Cardiff-1, modified from Bryant and Bartlett (1991). This figure shows location of the K3E sandstone reservoir and overlying and interbedded coaly source rocks (black in lithology log). Figure not to scale.

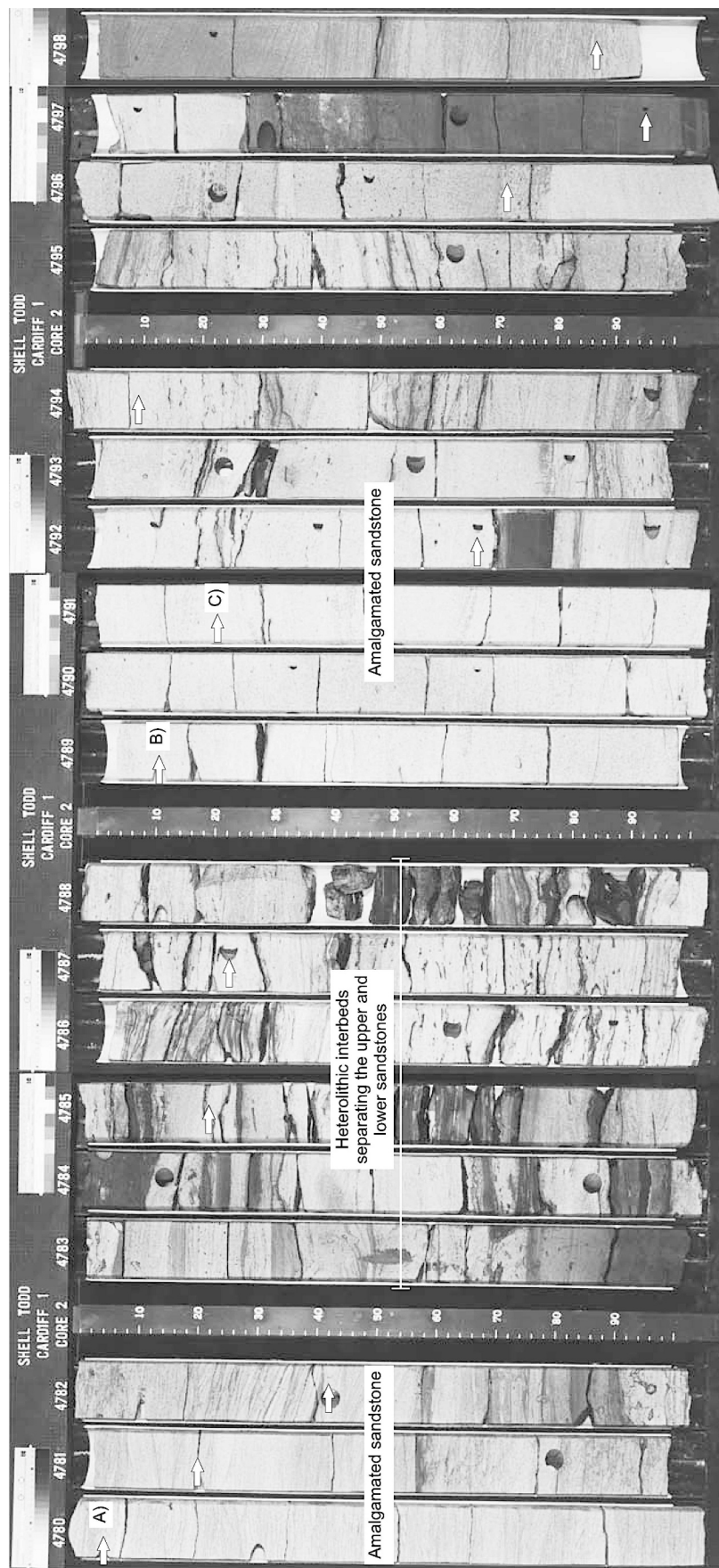


FIG. 3.—Core photographs from Cardiff-1 (Core Laboratories 1992) showing the position and lithology of petrographic samples (arrows) and samples for advanced analyses (A, B, and C).

permeability, respectively) despite fair to moderate measured porosity values (6.6–14.2%). Porosity determination was by helium injection, and permeability to air under unstressed conditions (Core Laboratories 1992).

Organic Geochemistry

Source-rock and maturity studies were not performed on Cardiff-1 samples, but evidence for a mature kitchen in this region is provided by the proven charge at Cardiff and surrounding structures. Potential source rocks are Late Cretaceous coals from the Rakopi Formation (King and Thrasher 1996) and intraformational coaly beds within the Paleocene–Eocene Kapuni Group.

Gas peaks detected by gas chromatography during mud logging of Cardiff-1 include C₁–C₄ components and significant gas levels whilst drilling Mangahewa coals. Some cuttings of coal tested positive for cut fluorescence, suggesting that generated oil was contained in the coal (STOS 1992).

The best gas shows in the K3E interval come from depth interval 4777–4803 m, peaking at 12% where core 2 was taken (STOS 1992). Natural even, dull yellow fluorescence was persistently present in the K3E interval, which sporadically gave a weak, milky white crush cut. Core 2 shows consistently even, moderate, blue-white natural fluorescence in the zones of best permeability. Some coals were noted to have a moderate, milky white cut fluorescence (STOS 1992; not recorded on mudlog), indicating they have entered the oil window and are early mature for oil.

METHODOLOGY

Twelve sandstone samples were selected for petrographic analysis from core 2 (K3EU reservoir) at Cardiff-1 (arrows in Fig. 3), with detailed analyses undertaken on three of these samples (labeled A, B, C in Fig. 3). The petrographic samples display a range in porosity and permeability values from 8.7% to 12.7% and 0.14 mD to 1.90 mD, respectively (Fig. 4). Samples were chosen in order to get a representative selection of laminated, massive, and disrupted sandstones through the fairly limited cored reservoir section (19 m).

Petrographic Analysis

All twelve samples were analyzed using transmitted-light microscopy on impregnated and stained thin sections (stained for K-feldspar and carbonate). Impregnation was undertaken in a vacuum to remove gas from the samples; samples were dried at 50°C and the epoxy was cured at 40°C. Modal point-count analysis was undertaken on all samples to investigate grain size (100 counts per section), mineralogy (300 counts per section), and pore type and pore volume (1000 counts per section).

Scanning electron microscopy (SEM) was undertaken on selected samples, providing additional information on the pore-system geometry, authigenic mineralogy, and paragenetic relationships. The analysis was undertaken on gold coated, freshly broken samples glued onto aluminum stubs. The SEM was attached with an Energy Dispersive X-ray analysis system (EDX) and detector, which allows analysis at a specific spot of about 1 micron diameter or collects emissions from a specific line on the screen or the whole screen area.

Semiquantitative X-ray diffraction analysis was undertaken on the < 2 µm fraction and 2–6 µm fraction of three samples (A, B, C) to establish the clay mineralogy. Clay-fraction XRD analyses were run air-dried, after solvation with ethylene glycol vapor overnight, and after heat treatment at 350°C and 550°C for 2 hours duration.

Transmission electron microscopy (TEM) was undertaken on the three < 2 µm fractions in order to assess potential contamination of the clay separates by K-feldspar. A JEOL JEM 2010 200 kV TEM was used for detailed grain-by-grain morphological characterization of the < 2 µm clay fractions and for control of grain-size distribution within the

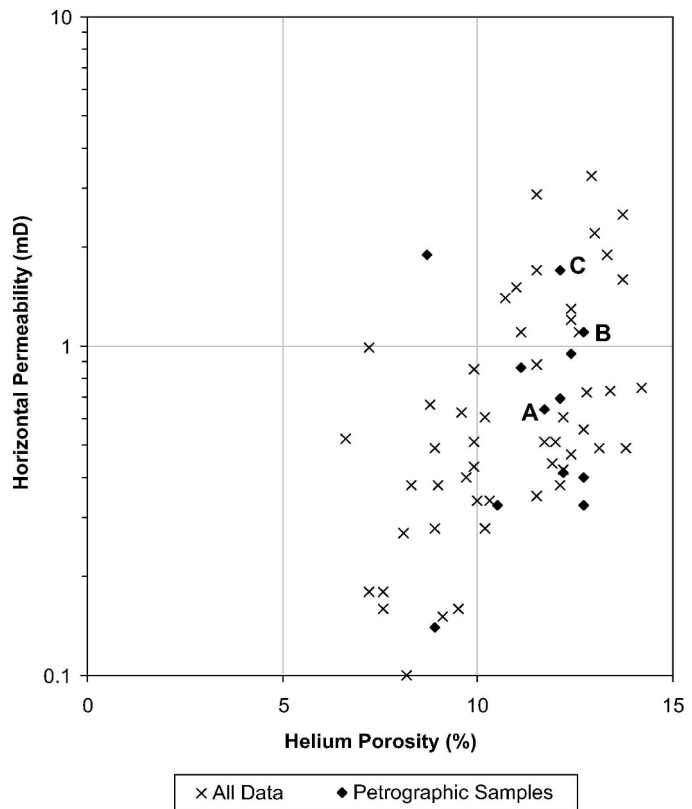


FIG. 4.—Graph of porosity versus permeability for core from Cardiff-1 (data from Core Laboratories 1992) showing the range of porosity–permeability values for petrographic samples.

fractions. Samples were prepared by placing one drop of clay solution on a micro carbon grid film and drying under air. The composition of individual particles was investigated by an attached EDS system.

K-Ar Dating

Authigenic illites were separated from the fines fraction of three samples (A, B, and C in Fig. 3) and analyzed for K-Ar age determination. All three samples for illite dating were crushed into chips by hammer (maximum dimension < 10 mm) and then gently disaggregated by using a repetitive freezing and thawing technique to avoid artificial reduction of rock components and contamination of finer size fractions with K-bearing minerals such as K-feldspar (Liewig et al. 1987). Grain-size fractions of < 2 µm and 2–6 µm were separated in distilled water according to Stokes' law, and the efficiency of this separation was monitored by SEM. No apparent flocculation was observed during the clay separation procedure.

Potassium content was determined by atomic absorption (Varian Spectra AA 50) using Cs at 1000 ppm concentration for ion suppression. 100–200 mg sample aliquots were dissolved with HF and HNO₃ (Heinrichs and Herrmann 1990). Once in solution, the samples were diluted to 0.3 to 1.5 ppm K for the atomic absorption analysis.

Argon isotopic determinations were performed using a procedure similar to that described by Bonhomme et al. (1975). Samples were preheated under vacuum at 80°C for several hours to reduce the amount of atmospheric Ar adsorbed onto the mineral surfaces during sample handling. Argon was extracted from the separated mineral fractions by fusing samples within a vacuum line serviced by an on-line ³⁸Ar spike pipette. The isotopic composition of the spiked Ar was measured with

a high sensitivity on-line VG3600 mass spectrometer, and the ^{38}Ar spike was calibrated against international standard biotite GA1550 (McDougall and Roksandic 1974). After fusion of the sample in a low blank Heine resistance furnace, the released gases were subjected to a two-stage purification procedure with a CuO getter for the first step and two Ti getters for the second step. Blanks for the extraction line and mass spectrometer were systematically determined, and the mass discrimination factor was determined periodically by airshots.

During the course of the study one international standard (1 LP-6) and one airshot value were measured. The pooled error of duplicate K determination on several samples and standards is better than 2%, whilst the error for Ar analysis is below 1.00% and the $^{40}\text{Ar}/^{36}\text{Ar}$ value for the airshot is 291.70 ± 0.20 . The K-Ar ages were calculated using ^{40}K abundance and decay constants recommended by Steiger and Jäger (1977). The age uncertainties take into account the errors during sample weighing, $^{38}\text{Ar}/^{36}\text{Ar}$ and $^{40}\text{Ar}/^{38}\text{Ar}$ measurements, and K analysis. K-Ar age errors are within 2 sigma uncertainty.

Analysis of Fluid Inclusions

Fluid inclusions were analyzed on three samples (A, B, and C in Fig. 3). Fluid inclusions within detrital and authigenic quartz were analyzed petrographically and microthermometrically on 100- μm -thick polished sections at magnifications of 400 \times , 500 \times , and 800 \times . The analyzed fluid inclusions range in diameter from 4 to 40 μm with a modal value of 8 μm .

Identification, classification and determination of relative paragenetic sequences and photography of inclusions was carried out under incident ultraviolet light (365 nm excitation filter) and/or transmitted white light using a Leitz petrographic microscope. Microthermometry of fluid inclusions was performed on a gas-flow heating and freezing stage mounted on the Leitz microscope. Air was used as a coolant during heating; liquid and gaseous nitrogen were passed through the device for freezing inclusions.

Burial History

A detailed burial history was generated for the Cardiff-1 site, utilizing well data and isopachs of deeper formations based on maps from Thrasher and Cahill (1990). Lithologies are based on the well report (STOS 1992), paleo-water depths from King and Thrasher (1996), and temperatures corrected from BHT data using the approach of Funnell et al. (1996).

Zetaware Genesis software (Zetaware Inc., Interactive Petroleum System Tools; Zetaware.com) was used to develop the 1D transient thermal model using a constant 38 mW/m 2 base-lithosphere heat flow. The present-day surface heat flow of 56 mW/m 2 comprises components from the crustal heat flow, a crustal radiogenic component of 20 mW/m 2 , and the effects of 850 m of recent uplift and denudation followed by 160 m of sediment burial. Estimates of heat flow are after Funnell et al. (1996), and estimates of uplift are after Armstrong and Chapman (1999).

A different organic richness was applied to the burial model for Paleogene and Cretaceous source-rock intervals. Total organic carbon (TOC) of 5% and a hydrogen index (HI) of 260 mg/g was used for Paleogene units, and 6% TOC and 300 mg/g HI was used for the Cretaceous Rakopi Formation (unpublished GNS data).

CO₂ kinetics applied in the model are from Burnham and Sweeney (1989); all other kinetic parameters are those published by Pepper and Corvi (1995a) for terrestrial, waxy, DE organic facies, which are considered most representative for Taranaki coaly source rocks (Sykes 2001). Note that oil is modeled as being expelled once 100 mg/g of oil generation is achieved, assuming a 100 mg/g saturation threshold as suggested by Pepper and Corvi (1995b). Hence, our models predict that these coaly source rocks start oil generation at about 100°C and oil

expulsion at about 135°C. The gas saturation threshold used in the model is 30 mg/g.

PETROLOGY

Petrographic results from Cardiff-1 are summarized in Table 2. Samples are moderately or moderately well sorted, with a medium or coarse mean grain size (243–689 μm) and classify as quartz arenites, subfeldsarenites, or sublitharenites using the classification scheme of Folk et al. (1970; Fig. 5). All samples are extremely quartz-rich, with most lithic fragments composed of quartz and variably clay-replaced subgrains. Other detrital grains are rare but include minor K-feldspar (< 5%) and locally minor plagioclase (< 3%), mica (< 2%), and heavy minerals (Table 2). This detrital composition suggests original derivation from an igneous source, possibly as recycled grains from another sedimentary formation.

Authigenic minerals are abundant, comprising significant illitic clay (14–24% including intercrystalline microporosity) and quartz overgrowth cements (6–16%). Semiquantitative XRD analysis of the < 2 μm and 2–6 μm fractions from three samples confirms that the fines are dominated by illite-rich (c. 90% illite), regular mixed-layer illite-smectite ($R = 3$ ordering; Table 3). Most of the illitic clay occurs as a very fine grain (or clay)-replacement phase (Fig. 6A, B), although significant illite also occurs as intergranular and grain-coating clays. Coarsely crystalline illitic flakes and booklets are also present, and the morphology of these clays suggests formation by illitization of kaolinite (Fig. 6C, D); it is possible that much of the very fine grain (or clay)-replacement illite may also represent illitized kaolinite. Typically, only traces of unaltered kaolinite were identified in thin section, which is consistent with XRD results (Table 3). However, EDX analysis of platy and sheet-like illitic clays seen with the SEM (Fig. 6E, F) shows them to contain Al/Si ratios that could be consistent with alteration from earlier-formed kaolinite. Notably, the SEM also highlights the presence of fine fibrous illite, which is difficult to observe with transmitted-light microscopy (Fig. 6E, F). These sheet-like and fibrous morphological forms of illite are comparable to those described and interpreted as illitized kaolinite by other authors (e.g., Ehrenberg and Nadeau 1989; Storvoll et al. 2002).

Quartz cements occur in all the petrographic samples as partial euhedral overgrowths on detrital grains (e.g., Fig. 6E); no rounded or abraded overgrowths were observed, suggesting that the quartz cement has not been recycled from another sedimentary formation. The cements partially occlude secondary feldspar-dissolution pores (e.g., Fig. 6A, K) and enclose both authigenic clay minerals (Fig. 6B) and residual oil (Fig. 6I). Carbonate cements are relatively minor or absent in the samples analyzed (0–8%), occurring as pore-filling ferroan dolomite in seven samples and predominantly grain- and mud-replacing siderite in five samples.

Macropores (pores > 16 μm long) are fairly minor in the samples from Cardiff-1 (1–5%; Table 2) forming approximately 15–45% of the total measured porosity. In most cases, macroporosity has formed by secondary dissolution, and occurs either as isolated grain-dissolution pores or the grain-dissolution component of hybrid pores (Fig. 6G, H); intergranular macropores are only a minor component (Table 4). Average macropore size ranges from 35 μm to 113 μm , whilst the mean hybrid pore size ranges from 51 μm to 155 μm , locally reaching a maximum size of 490 μm (Table 4). These large macropores are likely to be connected by a highly tortuous system of microporosity associated with the abundant illitic clay minerals.

Residual oil has been observed in six samples, being most common at sample depths 4787.2 m and 4796.7 m. It occurs as a grain-coating and pore-lining phase (e.g., Fig. 6C, D) but also as a thin film impregnating some of the authigenic clay minerals.

TABLE 2.—Summary point-count data.

General Sample Information			Mean grain-size (µm)	Macro-pores (% ; > 16 µm)	IG	G-dis	Hybrid	Macropores (%)	IPV (%)	IGV (%)	Total Cements (%)	Quartz (%)	K-feldspar	Plagioclase (%)	Lithics (dom. Qz)	Degraded Grains (%)	Mica (%)	Heavy Mins (%)	Detratal Clays (%)	
Sample No.	Core Depth (m)	He. Porosity (%)	Horiz. Perme. (mD)	Macro-pores ; Macro-pores (%)	IG	G-dis	Macro-pores part	IG	G dis part	IPV	IGV	Total Cements	Quartz	K-feldspar	Plagioclase	Lithics (dom. Qz)	Degraded Grains	Mica	Heavy Mins	Detratal Clays (%)
4780.0	20	11.7	0.64	327	3.0	0.3	1.5	0.3	0.9	0.6	16	67.1	54.6	3.7	1.7	5.0	1.4	0.7	0.3	
4781.2	24	12.7	0.40	262	2.3	0.1	0.8	0.1	1.3	0.2	14	60.3	54.4	2.3	1.7	1.0	0.6	0.3	0.3	
4782.4	28	10.5	0.33	243	1.4	0.2	0.9	0.4	0.2	0.2	13	59.0	49.7	3.7	2.0	2.6	1.0			
4783.2	38	12.7	0.33	353	4.7	0.5	2.3	0.4	1.6	0.9	12	57.9	55.3	0.3	Tr	1.3	0.3	0.7		
4787.2	44	12.1	0.69	397	2.6	0.3	1.1	1.1	0.3	17	61.0	54.1	5.0	Tr	1.3	0.3	0.3	1.7		
4789.1	49	12.7	1.10	687	4.0	0.3	2.5	0.1	1.2	0.4	14	69.3	60.3	1.7	6.7	0.3	0.3			
4791.2	56	12.1	1.70	689	4.3	1.1	1.4	0.1	1.7	1.2	13	70.3	62.0	1.4	6.6	0.3				
4792.6	61	11.1	0.86	566	5.0	0.9	3.3	0.4	0.5	1.3	11	62.9	57.6	0.7	2.3	1.7	0.3	0.3		
4794.1	66	12.4	0.95	374	3.2	0.4	1.2	0.2	1.4	0.6	18	62.3	58.4	0.7	1.0	1.6	0.3	0.3		
4796.7	75	8.7	1.90	467	3.6	0.6	1.4	0.2	1.3	0.8	15	67.7	63.7	Tr	0.7	3.0	0.3		1.0	
4797.9	79	8.9	0.14	297	1.5	0.2	0.7	0.4	0.2	11	63.7	58.3	2.6	0.3	1.9	0.3	0.3	3.3		
4798.9	82	12.2	0.41	324	2.9	0.6	0.5	0.2	1.5	0.8	13	61.3	59.1	1.0	0.6	0.3	0.3	1.0		

Authigenic Clay Minerals (%)			Illitic Clay						Total						Mineral Cements (%)						
Sample Depth (m)	Chlorite Total	Kaolin	2-fill	Int	2/rep	Int	2/rep	Int	Psu	G-C	G-rep	Int	2-fill	Int	2/rep	G-C	G/M-rep	Siderite	Anatase	Pyrite	Hydrocarbons (%)
4780.0	20.3											9.3	4.3	1.7	Tr	1.0				2.3	
4781.2	20.4											16.5	6.3	3.7	Tr	0.3	4.3			1.3	
4782.4	24.0											15.7	6.0	1.7	Tr	1.3	5.0			0.3	
4783.2	19.3	0.7	3.3	1.0	3.7	0.7	1.0	1.0	9.0	18.1	3.7	5.0	0.7	2.0	0.7	0.7			Tr	6.0	
4787.2	20.2											14.6	8.3	4.0	0.7	0.3	1.3				1
4789.1	15.0		Tr	Tr	0.3	1.3	1.3	2.3	9.7	11.7	8.0	3.7	0.3	0.3	1.3					Tr	
4791.2	14.1											11.4	8.7	2.7	0.0						Tr
4792.6	15.7											16.4	6.7	9.7							
4794.1	17.6	0.3										16.9	11.3	4.7	0.3	0.3					
4796.7	15.0											12.6	7.0	4.3	0.7	0.6	1				
4797.9	24.7											15.0	6.3	3.3	0.7	0.6					0.7
4798.9	13.7											20.9	6.3	3.7	1.3	7.0	0.3	2.3			

Note: microporosity has not been removed from counts of grains, authigenic clay minerals, or cements.

He. Porosity	Helium injection porosity	Int	Intergranular-filling
Horz. Perme.	Horizontal permeability to air (unstressed conditions)	2-fill	Secondary pore-filling
IG	Intergranular	2/rep	Secondary pore-filling/grain-replacive
G-dis	Grain dissolution	G-rep	Grain-replacive
IPV	Intergranular pore volume (IG + IG part hybrid)	G-C	Grain-coating
IGV	Intergranular volume as defined by Houseknecht (1987)	Psu	Pseudomatrix
		G/M-rep	Grain/mud-replacive

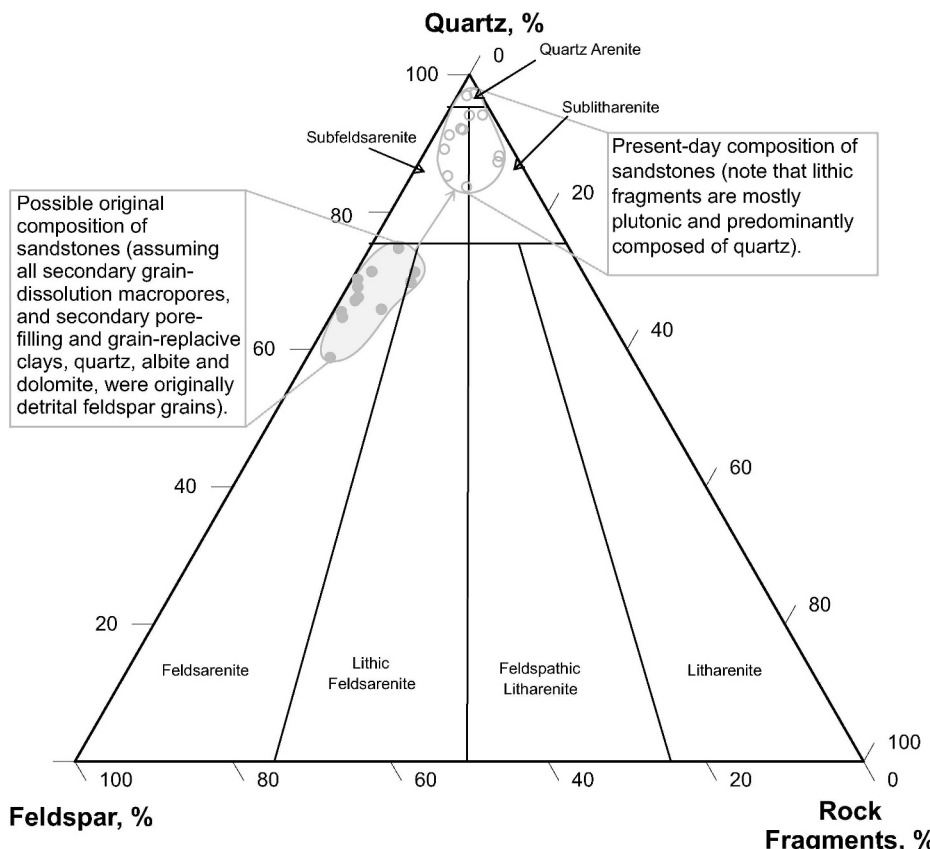


FIG. 5.—Ternary plot showing present-day composition of sandstones from Cardiff-1 and postulated original sandstone composition (using sandstone classification scheme of Folk et al. 1970).

COMPACTON

It is clear from petrographic observations that the sandstones from Cardiff-1 have undergone severe porosity reduction by compaction. Intergranular porosity is rare, and the calculated intergranular volumes (IGV; Table 2) are very low (mean c. 15%), as may be expected for such deeply buried samples. It has been suggested by other authors that porosity reduction is controlled mainly by mechanical compaction down to burial depths of 2.5–3.0 km (Ramm and Bjørlykke 1994) and that intergranular volume can potentially be reduced to 26% by mechanical compaction alone (i.e., a 35% reduction of intergranular porosity assuming a sand composed of non-ductile grains that are fairly spherical and well rounded with depositional porosity of 40%; Houseknecht 1987). Any further compactional reduction in porosity would then be attained by chemical compaction. The depositional porosity of Cardiff-1 samples is estimated at c. 35% (using tables from Beard and Weyl 1973 for medium-grained, moderately sorted sandstones). Therefore, assuming a 35% reduction of this porosity by mechanical compaction (to 23% IGV), results suggest that approximately 8% porosity reduction has occurred in the Cardiff-1 samples by chemical compaction. The

predominance of long and concavo-convex grain-to-grain contacts observed in the samples is supportive of moderate chemical compaction. However, 8% chemical compaction is a little higher than expected, particularly given the locally extensive quartz cement, which has been suggested by several authors to terminate chemical compaction due to strengthening of the sandstone framework (e.g., Lander and Walderhaug 1999; Walderhaug 2000). Some error in the calculation presented here could be due to analytical error in determining the IGV (e.g., difficulty in distinguishing intergranular quartz overgrowths from detrital grains, and difficulty in determining the intergranular component of large hybrid pores from the grain-dissolution component) and/or an underestimated amount of mechanical compaction (e.g., the amount of intergranular porosity reduced by mechanical compaction could potentially be higher in moderately sorted sandstones compared to well sorted sandstones).

DIAGENETIC REACTIONS

Petrographic results suggest that the K3EU reservoir at Cardiff-1 has undergone fairly advanced diagenetic alteration. At the time of deposition, the sandstones probably had a feldsarenite or lithic feldsarenite

TABLE 3.—Semi quantitative XRD analysis ($\pm 10\%$).

Sample Depth	Fraction Size	Illite-smectite	Kaolinite	Chlorite	Quartz	Feldspar	Plagioclase
4780.0	< 2 μm	92	2		6		
4780.0	2–6 μm	78.4			12.6	6.7	2.3
4789.1	< 2 μm	90	.2		8		
4789.1	2–6 μm	72		3.9	16.8	7.3	
4791.2	< 2 μm	92	2		6		
4791.2	2–6 μm	86.5	1.1		10.2	2.2	

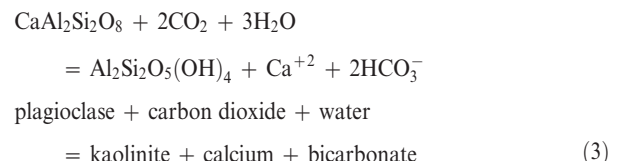
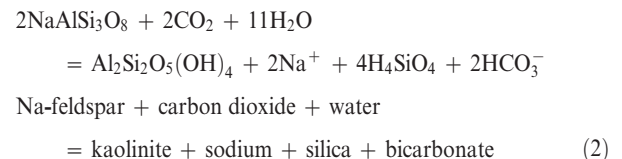
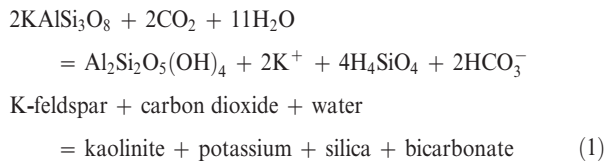
composition (Fig. 5). This depositional composition has been calculated assuming that all secondary grain-dissolution macropores and secondary pore-filling and grain-replacing minerals (i.e., clays and cements including microporosity) were originally detrital feldspar grains or feldspar subgrains within igneous lithic fragments. Making this assumption, approximately 21% of original feldspar (mean value from all samples) is thought to have undergone reaction. Evidence that significant feldspar has undergone reaction in the Cardiff-1 well is presented by the common occurrence of partially dissolved remnant grains within authigenic clays and/or secondary porosity (e.g., Figs. 6A, B, I, J). These feldspar reactions have resulted in generation of minor secondary porosity and significant precipitation of authigenic clay minerals, authigenic quartz, and associated intragranular and intercrystalline microporosity.

Feldspar reactions are likely to have taken place during several stages in the burial history, and may be related to circulation of acidic pore fluids through the reservoir. A very early, eogenetic phase may have occurred, related to fresh-water influx during or just after deposition within the fluvial to estuarine environment. However, the majority of feldspar reactions are thought to have occurred later during burial diagenesis. This is suggested by the presence of uncompacted secondary dissolution porosity and secondary pore-filling authigenic clays (e.g., Fig. 6G, H); any very early-formed porosity is likely to have been removed by the process of mechanical compaction, and early-formed clays would similarly have been squeezed into a pseudomatrix. In addition, feldspar dissolution occurring during eogenesis usually results in significant loss of silica and aluminum from the system (e.g., Bloch and Franks 1993), resulting in a net increase in secondary porosity compared to the volume of kaolinite and quartz precipitated. This is not consistent with results of mass balance presented later, providing further evidence that much of the feldspar reaction occurred during burial diagenesis.

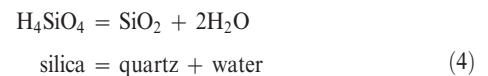
Paragenetic relationships observed in thin section suggest that there are two main stages for reaction during burial diagenesis (probably over a prolonged time period), associated with mineral authigenesis and/or porosity generation.

Stage 1 Burial Diagenesis

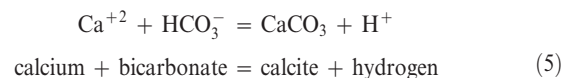
The first stage of burial diagenesis can be summarized as the reaction whereby detrital feldspar (reactant) reacts with acidic pore fluids to form kaolinite and minor quartz (products; e.g., Land 1984; Bjørlykke 1984; Siebert et al. 1984), along with the generation of some grain-dissolution porosity. Acidic fluids during burial can arise from dissolution of carbon dioxide into the porewater ($\text{CO}_2 + \text{H}_2\text{O} = \text{H}^+ + 2\text{HCO}_3^-$). Incorporating this into summary equations, the first stage of burial diagenesis observed at Cardiff-1 can be represented by the following:



Silica formed by the upper two reactions can precipitate authigenic quartz (e.g., Land 1984):



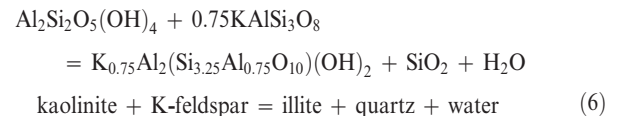
whilst bicarbonate formed by reactions 1–3 may react with available calcium and other ions to form carbonate cements (e.g., Land 1984):



The source of CO_2 that is driving reactions 1–3 is discussed later.

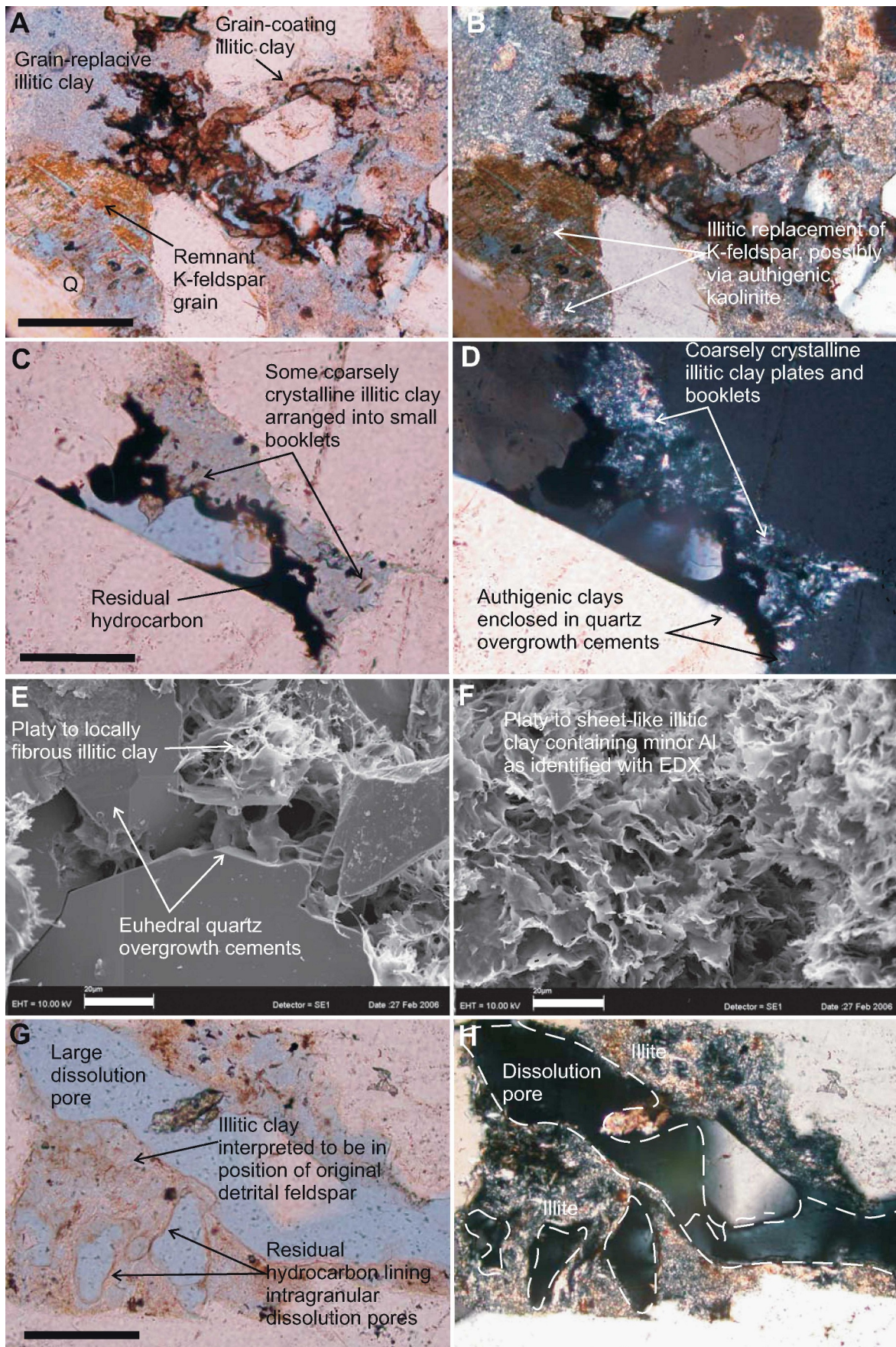
Stage 2 Burial Diagenesis

It is clear from petrographic observations that much of the kaolinite formed in stage 1 burial diagenesis has subsequently undergone alteration to illite. A source of potassium is required to form the illite, and this may have come from further dissolution of K-feldspar grains. This second stage in burial diagenesis can therefore be represented by the equation from Bjørlykke (1984):



The presence of authigenic illite within most grain-dissolution pores in the K3E sandstones at Cardiff-1 has resulted in a microporous system and highly tortuous pore network. However, some large and isolated dissolution macropores (with little internal evidence of illitization) are preserved. Illitization would have been most favorable where nucleation sites were available (e.g., as authigenic kaolin or other clays), whilst net dissolution may have remained at the sites of isolated dissolution macropores (i.e., where kaolinite or other clays had not precipitated). These pores are locally lined by residual oil, suggesting that they may have been preserved by oil-saturated porefluids (Fig. 6G, H). This could

FIG. 6.—Photomicrographs showing authigenic phases and paragenetic relationships. A, B) plane-polarized light (PPL) and cross-polarized (XP) views showing abundant authigenic illite occurring as a grain or clay replacement and grain-coating phase; note the presence of remnant detrital K-feldspar. Scale bar 170 μm . C, D) PPL and XP views of locally platy illitic clays, some of which are arranged into books, probably pseudomorphing earlier formed kaolinite. Scale bar 100 μm . E, F) SEM photomicrographs showing the occurrence of platy illitic clay and locally fine and filamentous illite; EDX analysis demonstrates that the platy illitic clay contains some Al. Scale bars 20 μm . G, H) PPL and XP views showing abundant authigenic illite occurring mostly as a grain or clay replacement; note the presence of large dissolution pores lined by oil-stained clays and completely devoid of illite. Scale bar 165 μm . I, J) PPL and XP views of quartz overgrowth cements enclosing residual oil; note also the grain-coating illitic clay. Scale bar 100 μm . K, L) PPL and XP views showing the local occurrence of thick quartz overgrowth cements within secondary grain-dissolution pores; note the thin film of residual oil lining the macropore. Scale bar 160 μm . M, N) PPL and XP views showing the etched remains of secondary pore-filling carbonate cement; note also the presence of authigenic illite, quartz, and some secondary dissolution macropores. Scale bar 145 μm .



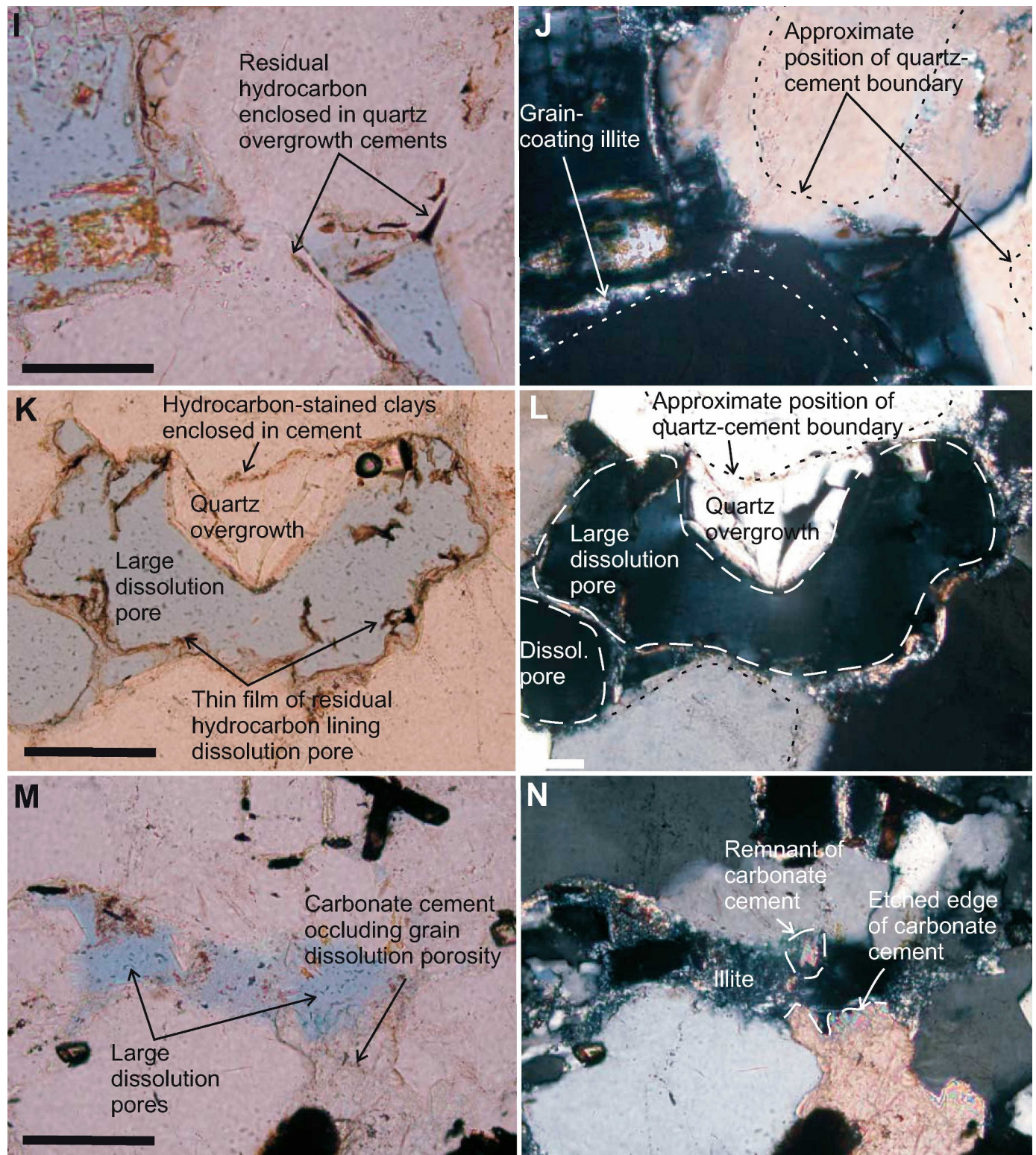


FIG. 6.—Continued.

explain the occurrence of some large, clay-free secondary pores, despite the typically pervasive nature of illitic clays elsewhere in the Cardiff-1 samples. It is therefore suggested that oil emplacement occurred before stage 2 burial diagenesis.

Enclosure of residual oil within authigenic quartz (Fig. 6I, J) and the location of overgrowths within large secondary dissolution pores (Fig. 6K, L), thought to have previously been occluded by oil, is evidence that a phase of quartz cementation also occurred very late in diagenesis, possibly in the second stage of burial diagenesis associated with illitization. However, given the evidence for chemical compaction, it is also likely that some of the silica sourcing very late-stage quartz cement has come from pressure solution at grain-to-grain contacts resulting from high burial temperatures and pressures.

It is difficult to ascertain timing of carbonate cements given that they are highly reactive. Bicarbonate is a product of several reactions proposed in stage 1 burial diagenesis (reactions 1–3), and this may react with available calcium and other ions to form carbonate cements (reaction 5). However, evidence for partial dissolution of carbonate cement has been observed from several thin sections (Fig. 6M, N), and it is likely that several dissolution and precipitation events have occurred, depending on the balance of pH and equilibrium reactions.

Mass Balance

Stage 1 of burial diagenesis at Cardiff-1 has resulted in the precipitation of kaolinite and quartz at the expense of detrital feldspar (equations 1–4). Bjørlykke (1984) has suggested that one volume of K-feldspar could form 60% kaolinite and 40% quartz. If we assume that c. 21% feldspar has undergone reaction (where total dissolution pore volume = grain dissolution macroporosity + grain-dissolution-filling cements and clays), then mass-balance calculations suggest that this feldspar could potentially have sourced 11% kaolinite and 7% quartz. From the point-counted data, an average 16% clays (excluding illitized mica, matrix, and chlorite) and 11% quartz cement gives a surprisingly similar ratio (60:40) but would require slightly more grain reaction (c. 27% feldspar dissolution) than indicated by present-day volume of secondary porosity, clay and cement (21% mean value from samples). This discrepancy can be accounted for in a number of ways: (1) clays contain significant intercrystalline microporosity, and therefore the true mean volume of clay will be lower than the mean 16% measured; (2) authigenic quartz has had an additional late source from pressure solution at grain–grain contacts; (3) present-day products (clays and quartz) probably have resulted from both stage 1 and stage 2 reactions; (4) analytical errors, which are likely to be greater than $\pm 1\%$. Despite the uncertainties, it can be concluded that mass-balance calculations support a feldspar source of ions for reaction and that the reasonable balance suggests a relatively “closed” diagenetic system.

K-AR DATING

Authigenic illite in sandstones contains potassium, which is suitable for age determination using the potassium-argon (K/Ar) geochronometer. Diagenetic illite is of interest for the petroleum industry because it can provide a K-Ar date constraining a heating and/or fluid flow event within a sedimentary basin (Pevear 1999). Dating of K-bearing illite minerals, using the K/Ar isotopic systems, has been undertaken on K3E reservoir sandstones at Cardiff-1 to establish the absolute timing of diagenetic events. Results from K-Ar dating of the $< 2 \mu\text{m}$ and $2\text{--}6 \mu\text{m}$ fractions of illites are presented in Table 5.

The K-Ar dates for the $< 2 \mu\text{m}$ fraction are fairly comparable between the three analyzed samples, with the youngest age (4.34 Ma) derived from sample 4789.1 m and the oldest age (6.79 Ma) derived from sample 4780.0 m. It is unlikely that the difference in age relates to a variation in the timing of illitization. It is more likely that the difference relates to

minor detrital illites that were included in the $< 2 \mu\text{m}$ separate, with more detrital clay identified in the uppermost sample (4780.0 m) compared to the lower two samples. Detrital illites will have a significantly older age than the authigenic illite, and therefore mixture of detrital and authigenic clay would result in an apparently older illite age.

XRD analysis indicates that the $< 2 \mu\text{m}$ separate does not contain K-feldspar (Table 3), which can be a major source of contamination of authigenic illites. Transmission electron microscopy (TEM) with an attached EDS system has also been used in this study to identify and distinguish authigenic clays from contaminants, by individual grain analysis, for purity control as proposed by Hamilton et al. (1992). Typical TEM images of illite grains are illustrated in Figure 7. TEM observations of the separated clay fractions document the occurrence of two distinct groups of particles: (1) idiomorphic illite fibers with elongated, well crystallized grain edges and (2) idiomorphic platy illite flakes, together with minor amounts of hexagonal idiomorphic kaolinite with clear crystallized edges. Traces of electron-dense dark particles could be identified within the $< 2 \mu\text{m}$ fractions as Ti-rich accessory minerals (e.g., Fig. 7B), but these do not contain potassium for contamination. No K-feldspar contamination could be identified in the $< 2 \mu\text{m}$ fractions by TEM, and therefore the K-Ar range of 4.34 to 6.79 Ma is considered realistic.

K-Ar dates for the larger size fraction ($2\text{--}6 \mu\text{m}$) yields older ages of between 13.1 Ma and 15.7 Ma (average c. 14 Ma). XRD results suggest that potassium in the $< 2 \mu\text{m}$ fraction is derived exclusively from illite (hence no feldspar contamination), whilst potassium in the $2\text{--}6 \mu\text{m}$ fraction comes predominantly from illite, but with a small component from feldspar (Table 3). It is therefore likely that the older K-Ar ages from the coarser fraction are largely due to contamination from feldspar; it would require only a few percent of Cretaceous-derived detrital feldspar (cf. Smale 1996) to result in a K-Ar age of c. 13 Ma when mixed with authigenic illites with a true age of c. 5 Ma. However, it is also possible that the $2\text{--}6 \mu\text{m}$ size fraction may have formed at an earlier stage than the finer ($< 2 \mu\text{m}$) size fraction. For neocrystallized illite, the finest separated particle size is derived from the ends of filamentous grains and should represent the most recently grown illite in sedimentary rocks. Conversely, coarser size fractions formed earlier during the illite formation process should (and do) yield older ages. It is therefore possible that the grain-size fractions of newly grown illite are mixtures of illite particles formed at different times during growth.

In summary, the comparable K-Ar age from the $< 2 \mu\text{m}$ fraction of illites from samples 4789.1 m and 4791.2 m suggests that the timing of fine illitization within the K3E reservoir at Cardiff-1 was in the early Pliocene at c. 4.5 Ma. XRD and TEM observations from the $< 2 \mu\text{m}$ fraction confirm that the fractions are clean and comprise mainly elongated well crystallized authigenic fibrous illite. The older age derived from coarser illite fractions ($2\text{--}6 \mu\text{m}$) is probably due to contamination (from feldspar and possibly also detrital illite and mica), but would also be consistent with illitization starting earlier than 5 Ma. It is therefore considered here that the $< 2 \mu\text{m}$ fraction reports the maximum age of illite growth. This is in accordance with Lee et al. (1985), who suggest that $< 2 \mu\text{m}$ K-Ar illite ages should be interpreted as maximum ages representing the main timing of illitization. The maximum-ages concept approximates the timing of main of illite growth (Meunier and Velde 2004).

FLUID-INCLUSION ANALYSIS

Primary and pseudosecondary fluid inclusions have been observed within detrital quartz grains, healed fractures (within detrital quartz), the dust rim between grain and overgrowth, and in overgrowth cements (Fig. 8A, B). Four major fluid-inclusion types have been identified: aqueous, oil, gas, and bitumen (Table 6). The most common, found in nearly all quartz grains, are aqueous fluid inclusions (Type 1), ranging

TABLE 4.—Pore characterization of samples from Cardiff-1.

Sample Depth	Total Macropores		Intergranular Pores		Grain-Dissolution Pores		Hybrid Pores (contain an intergranular and grain-dissolution component)			
	Mean Size	Max Size	Relative % of total	Mean Size	Relative % of total	Mean Size	Relative % of total	Intergranular component as relative % of hybrid	Grain-dissolution component as relative % of hybrid	Mean Size
4780.0	37 μm	100 μm	10%	10 μm	50%	31 μm	40%	25%	75%	51 μm
4781.2	62 μm	195 μm	4%	10 μm	35%	41 μm	61%	7%	93%	77 μm
4782.4	50 μm	150 μm	12%	15 μm	62%	43 μm	26%	0	100%	86 μm
4785.2	41 μm	120 μm	10%	11 μm	48%	34 μm	40%	20%	80%	55 μm
4787.2	76 μm	485 μm	13%	12 μm	42%	31 μm	45%	3%	97%	136 μm
4789.1	63 μm	310 μm	7%	27 μm	62%	55 μm	31%	7%	93%	87 μm
4791.2	61 μm	225 μm	25%	21 μm	32%	53 μm	43%	7%	93%	91 μm
4792.6	38 μm	140 μm	17%	14 μm	65%	34 μm	18%	40%	60%	72 μm
4794.1	62 μm	170 μm	11%	11 μm	36%	42 μm	52%	13%	87%	87 μm
4796.7	113 μm	490 μm	18%	18 μm	39%	75 μm	43%	14%	86%	155 μm
4797.9	35 μm	110 μm	14%	10 μm	57%	26 μm	29%	0	100%	65 μm
4798.9	70 μm	310 μm	22%	11 μm	17%	34 μm	61%	14%	86%	102 μm

from monophase (liquid; Fig. 8C) to two-phase (vapor + liquid; Fig. 8D) at room temperature. Oil (Type 2) inclusions have only been observed in the lower two samples (4789.1 m and 4791.2 m) and are subdivided into several groups depending on the number and type of phases present in the inclusion (Table 6). They include two-phase (vapor + oil) inclusions (Fig. 8E, F), three-phase (vapor + oil + aqueous solution) inclusions (Fig. 8G) and three-phase gassy aqueous inclusions with orange-brown colored daughter minerals (Fig. 8H) or bitumen. Gas inclusions (Type 3) are also observed only in the lower two samples; they may be either two-phase (Fig. 8I) or three-phase (Fig. 8J) at room temperature. Monophase bitumen inclusions (Type 4; Fig. 8K) are relatively rare.

Type 1—Aqueous Inclusions

The relative volume of the vapor bubble in two-phase fluid inclusions ranges from 1% to 16% with the majority clustering at 5%. Most of the aqueous fluid inclusions contain high concentrations of dissolved gas (very few are gas-free) and form clathrates when frozen (Roedder 1984). Clathrates affect the freezing-point depression temperatures and mask true salinities of the entrapped solutions. Even low concentrations of gas can affect salinity measurements by lowering the temperature of last ice melting (T_m) and result in apparently high calculated salinities (Hedenquist and Henley 1985). Most clathrates in aqueous solutions in Cardiff-1 dissolve at $< 10^\circ\text{C}$, suggesting the presence of dissolved CO_2 (cf. Roedder 1984).

Homogenization data were acquired for aqueous fluid inclusions within assemblages, or arrays. All aqueous inclusions homogenize to the liquid phase. Data on homogenization temperature (Th) are summarized in Figure 9 and below:

- Aqueous inclusions in the dust rim (at the contact between the detrital quartz and overgrowth) homogenize at 120 – 130°C for sample 4780.0 m.
- Aqueous inclusions within the overgrowths homogenize at about 105°C (100 – 120°C) for sample 4780.0 m.
- Aqueous inclusions in both the dust rim and overgrowth have overlapping homogenization temperatures for samples 4789.1 and 4791.2 m; Th peaks at 130°C (105 – 135°C).
- Primary inclusions and inclusions in healed fractures within the detrital quartz (mid-grain aqueous inclusions) homogenize at 155°C , 160 – 165°C , and 150°C for the three samples (4780.0 m, 4789.1 m, and 4791.2 m, respectively).

Salinity measurements were undertaken for aqueous inclusions, but most data is considered unreliable because of the high concentrations of dissolved gas (forming clathrates when frozen). The salinity of gas-free aqueous fluid inclusions from grain edge and overgrowth was measured at approximately 7700 mg/kg Cl equivalent.

Density calculations (which are required for pressure corrections of Th to trapping temperature, Tt) were not undertaken because of the gassy nature of most fluid inclusions and hence unreliable salinity measurements. However, it is generally assumed that if an aqueous solution was saturated with respect to gas at the time of trapping, the Th may approach or equal the temperature of trapping and therefore pressure corrections are not required (Hanor 1980). This could be the case at Cardiff-1, and the measured homogenization temperatures of gassy aqueous inclusions are therefore considered to be good estimates of actual entrapment temperatures (cf. Tseng and Potoroff 2002).

Type 2—Oil Inclusions

Oil inclusions have been subdivided into three groups (Table 6). Two-phase oil inclusions at 4789.1 and 4791.2 m have yellow and blue- to

TABLE 5.—*K-Ar dates for the < 2 μm fraction.*

Sample	Fraction Size	K [%]	Rad. 40Ar [mol/g]	Rad. 40Ar [%]	Age [Ma]	Error [Ma]	Period-Epoch-Age
4780.0 m	< 2 μm	6.83	8.0552E-11	40.13	6.79	0.22	Neogene-late Miocene-Messinian
4780.0 m	2–6 μm	6.33	1.7329E-10	90.36	15.71	0.32	Neogene-mid Miocene-Langhian
4789.1 m	< 2 μm	6.61	4.9871E-11	24.96	4.34	0.17	Neogene-early Pliocene-Zanclean
4789.1 m	2–6 μm	5.99	1.4269E-10	82.19	13.68	0.30	Neogene-middle Miocene-Serravallian
4791.2 m	< 2 μm	6.58	5.5836E-11	33.79	4.89	0.13	Neogene-early Pliocene-Zanclean
4791.2 m	2–6 μm	6.32	1.4408E-10	85.38	13.10	0.28	Neogene-middle Miocene-Serravallian
LP6 (#66) standard		8.37	1.9263E-09	96.25	128.03	1.86	N/A; Error: + 0.10% to reference

bluish-yellow-fluorescence under UV light. They were observed only in samples where streaming cut fluorescence was reported (Table 7). At 4780.0 m, where there was no cut fluorescence, oil inclusions occur only in feldspars, with none in quartz.

Three-phase vapor–oil–aqueous solution inclusions were not observed in quartz cements and occur only in the dust rim between the detrital grain and its overgrowth or in fractures confined within detrital quartz.

Three-phase inclusions with daughter minerals (orange-brown color) were found at 4789.1 m, in a healed fracture truncated by quartz overgrowth cement. The fluid inclusion homogenizes to the liquid phase at $125 \pm 2^\circ\text{C}$. The aqueous solution contains dissolved gas, indicated by the temperature of last ice melting at 3.0°C . The daughter mineral has a melting point of 2.8°C , often becoming colorless at about 125°C , and apparently homogenizes at $> 125^\circ\text{C}$.

Homogenization temperature data from oil and aqueous inclusions cannot be directly compared due to the different PVT properties of oil and brine, and has not been used in this study because the original composition of the pore fluid is unknown. However, the trapping temperature of oil inclusions can be inferred by comparison with homogenization temperature data from associated aqueous fluid inclusions. These data are summarized below:

- Two-phase (gassy) aqueous fluid inclusions found in the same healed fractures that cut across quartz overgrowths as two-phase oil inclusions homogenize to the liquid phase at $117 \pm 2^\circ\text{C}$.
- Two-phase (gassy) aqueous fluid inclusions associated with oil inclusions in healed fractures homogenize at c. $135 \pm 2^\circ\text{C}$.
- Two-phase (gassy) aqueous inclusions associated with the daughter mineral-bearing inclusions homogenize to the liquid phase at $125 \pm 2^\circ\text{C}$.

Type 3—Gas Inclusions

Gas inclusions are associated with aqueous fluid inclusions that homogenize at about 135°C (grain edge and overgrowth) and at 165°C (mid-grain, detrital). A few of the gas inclusions contain CO_2 , characterized by a triple point and critical-point temperatures near that of one-component CO_2 fluid (-56.6°C and near 31°C , respectively; cf. Roedder 1984), but these are likely to represent inherited gas from the quartz grains. Other gases are unidentified but are most likely an admixture containing methane (e.g., Burcik 1979). These gases have critical-point temperatures of 9 to 10°C and 2.5°C .

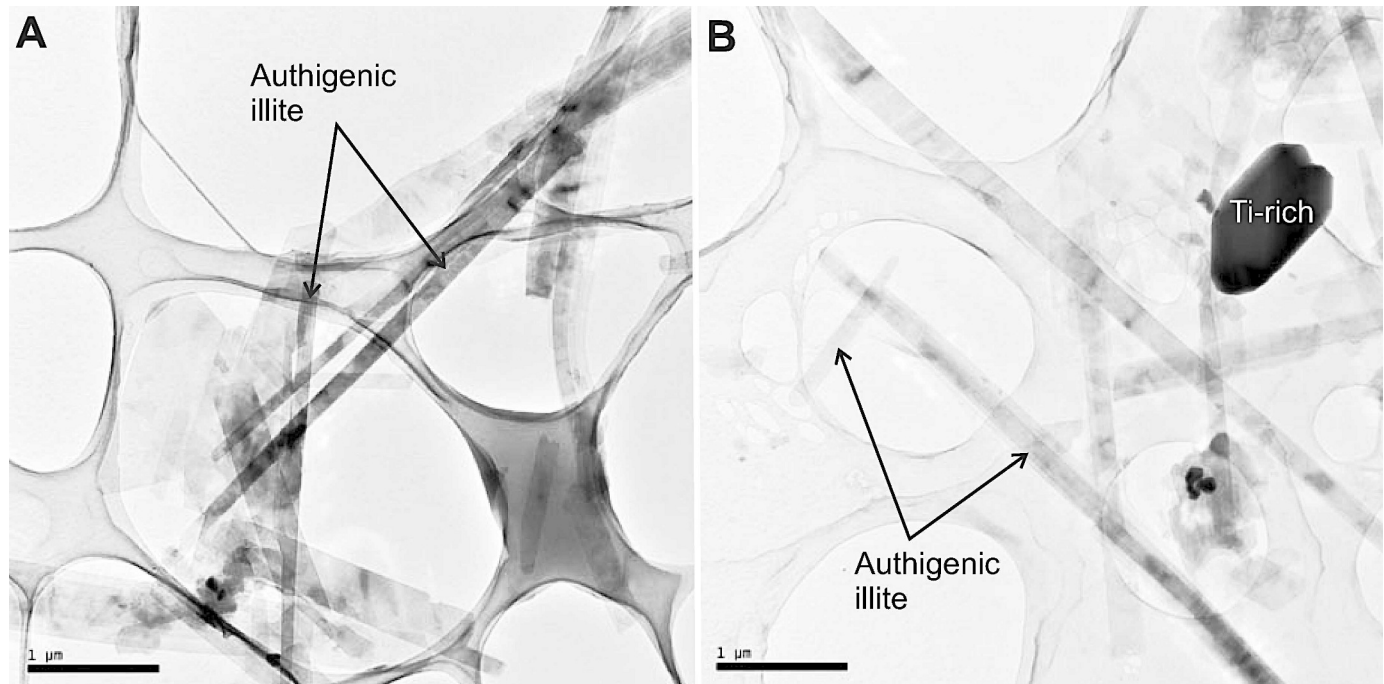


FIG. 7.—TEM photomicrographs of the < 2 μm size fraction. A) Dominant elongated, well crystallized authigenic illite. B) Well crystallized authigenic illite with minor contamination by a Ti-rich accessory mineral. Scale bars 1 μm.

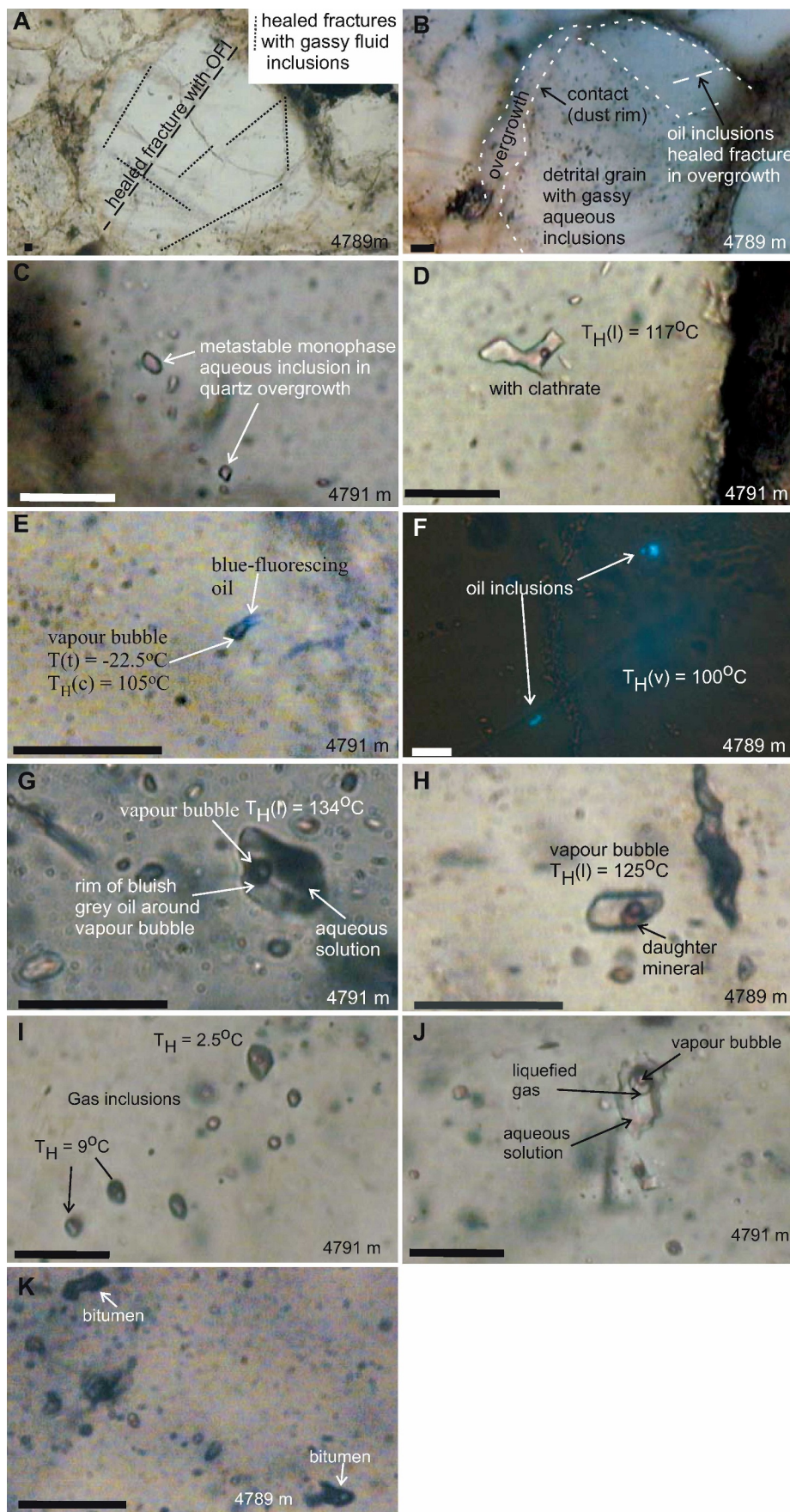


FIG. 8.—Photomicrographs of fluid inclusions. A) Crosscutting trails of healed fractures containing oil (OFI) and gassy aqueous inclusions. Note how the trail of OFI cuts across detrital grain and overgrowth. B) Gassy aqueous inclusions occur in the detrital grain and in the dust rim; oil inclusions occupy a healed fracture in the overgrowth. C) Metastable monophase high-gas aqueous inclusions in overgrowth with homogenization temperature (T_h) of 117°C . D) Two-phase gassy aqueous inclusion at 4791.2 m in overgrowth with $T_h = 117^\circ\text{C}$. E) Gassy oil inclusion (gas condensate) at 4791.2 m with triple-point temperature $T(t)$ of -22.5°C and homogenization temperature to the critical point ($T_h(c)$) at 105°C . F) Oil inclusions under UV light found in the healed fracture in photo A that homogenize to the vapor phase ($T_h(v)$) at 100°C . G) Three-phase vapor-oil-aqueous solution inclusion, where $T_h(l)$ is 134°C . H) Aqueous inclusion with brown daughter mineral. Aqueous solution has $T_h(l) = 125^\circ\text{C}$. I) Liquefied gas inclusions with apparent $T_h(l) = 2.5^\circ\text{C}$ and 9°C . J) Three-phase inclusion consisting of vapor bubble, aqueous solution, and liquid gas at 4791.2 m. K) Bitumen-filled inclusions associated with gassy aqueous inclusions. Scale bar = $20 \mu\text{m}$.

TABLE 6.—Description of fluid-inclusion types in Cardiff-1.

Type	Description	T_H (°C)	Comments
1	Aqueous fluid inclusions ■ Monophase aqueous ■ Two-phase (vapor + aqueous solution)	100 to > 190	Often forms clathrates indicating high % of dissolved gas
2	Oil inclusions ■ Two-phase oil and gas condensate (vapor + oil) ■ Three-phase (vapor + oil + aqueous solution) ■ Three-phase (vapor + aqueous solution + daughter mineral)	63-150	Two-phase oil inclusions homogenize to the liquid or vapor phases. Three-phase gas condensate inclusions homogenize to the critical point by meniscus disappearance.
3	Gas inclusions ■ Two-phase (vapor + liquefied gas) ■ Three-phase (vapor + liquefied gas + aqueous solution)	2.5-31	
4	Monophase bitumen (solid)		Often associated with gassy fluid inclusions in healed fractures

Type 4—Bitumen Inclusions

Monophase bitumen inclusions often occur in healed fractures, associated with gassy aqueous fluid inclusions. The bitumen appears as a black solid that often has a bluish to grayish fluorescence under UV light. The close association between bitumen-bearing inclusions and gassy

aqueous fluid inclusions in healed fractures suggests that some of the black solids are probably resins and asphaltenes.

Paleo-Oil Column

A technique similar to the GOI of Lisk et al. (1998) was used here to determine the likelihood for a paleo-oil column at Cardiff-1. This technique measures the relative proportion of different types of fluid inclusions as ratios of point-counted abundances. Quartz grains containing gassy saline solutions are subsets of aqueous inclusions, with the percentage of quartz grains with gassy fluid inclusions ($G\%$) calculated by

$$G\% = (Q_g/n_a) * \%aq \quad (7)$$

where Q_g = number of quartz grains containing gassy inclusions; n_a = total number of quartz grains, in a section, containing aqueous inclusions; $\%aq$ = total percentage of quartz grains containing aqueous inclusions in the section.

The total number of quartz grains that contain oil-filled inclusions (OFI) is expressed as

$$\%OFI = (\text{number of quartz grains with oil inclusions} * 100)/n \quad (8)$$

where n = total number of quartz grains counted.

Quartz grains containing inclusions of bitumen were also point-counted and expressed in percentage similar to OFI%, where

$$\text{Bitumen}\% = (\text{number of quartz grains with bitumen} * 100)/n \quad (9)$$

The average OFI, bitumen, and gassy indices are presented for each sample depth in Table 7 and Figure 10.

Significant OFI% values are > 5%, indicating moderate to high paleo-oil saturation (Lisk et al. 1998, where OFI% is comparable to GOI of Lisk et al. 1998). Of the three samples counted at Cardiff-1, moderate paleo-oil saturation occurs only at 4791.2 m, where the OFI% is 16%. There is a positive correlation between OFI% and bitumen% (Fig. 10), showing that both oil inclusions and bitumen inclusions within quartz grains are most abundant in sample 4791.2 m, minor in sample 4789.1 m, and absent or rare (respectively) in sample 4780.0 m. These data would be consistent with a possible paleo-oil column below c. 4790 m depth (where the OFI is 16%), although more data points are required to confirm this. Fluorescence data from this interval also points to the presence of present-day petroleum in rock pores (Table 7). Oil cuts observed during drilling suggest a continuum between the paleo-oil charge(s) recorded in the inclusions and the present-day oil that resides in pore spaces.

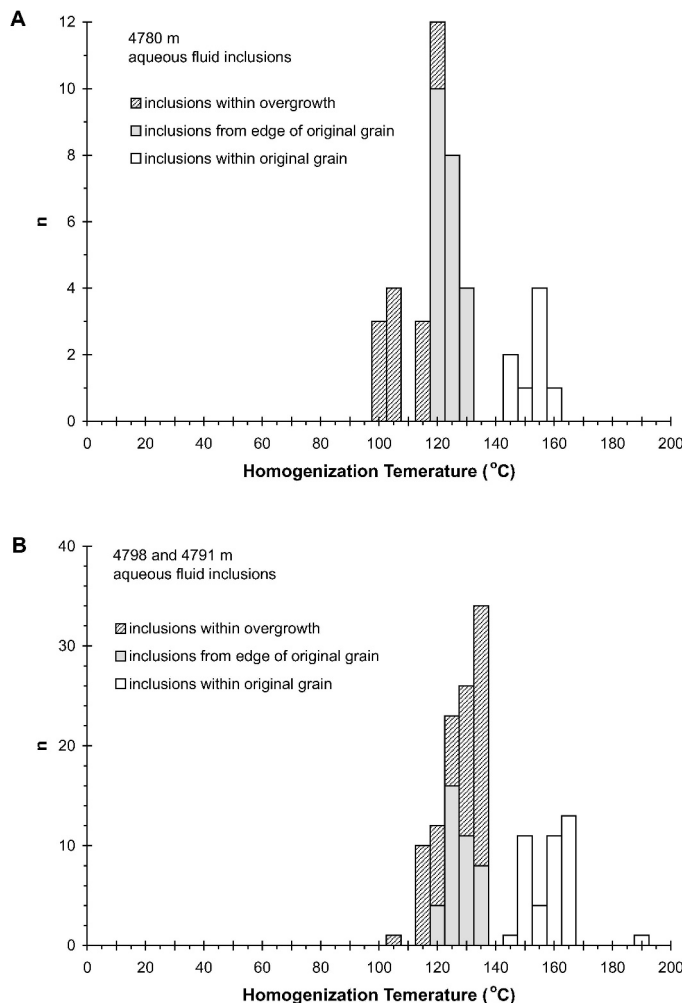


FIG. 9.—Homogenization temperatures of aqueous fluid inclusions at A) 4780.0 m and B) gas and aqueous fluid inclusions at 4789.1 and 4791.2 m. Homogenization temperatures for inclusions found within the detrital quartz crystal (1) the dust rim between detrital quartz and overgrowth (2) and within overgrowths or cutting across overgrowth and detrital grain (3) are shown.

BASIN MODEL AND MATURATION HISTORY

The burial-history model for Cardiff-1 shows a variable rate of burial and variable paleo-bathymetry (Fig. 11). Coastal-plain through to

TABLE 7.—Megascopic fluorescence and percentages of quartz grains containing oil inclusions (OFI%), bitumen and gassy solutions (Gassy%) in Cardiff-1 samples.

Depth (m)	Lithology	Megascopic Fluorescence ¹	OFI %	Bitumen %	Gassy %
4780.0	Subfeldsarenite	70% dull yellow-gold direct fluorescence, no cut fluorescence	0.0	2.2	55
4789.1	Sublitharenite	95% even bright yellow-white direct fluorescence, moderate white streaming cut	3.4	7.4	43
4791.2	Sublitharenite	100% even bright yellow to blue white direct fluorescence, 50% yellow, 50% blue-white, moderate white streaming cut	16.2	42.7	29

shallow marine environments dominated the onshore Taranaki region during the Late Cretaceous and Paleocene–Eocene, with increased water depth into the Oligocene. This was followed by a period of rapid burial during the early to mid Miocene that reflects basin-wide subsidence (King and Thrasher 1996) associated with relatively high sedimentation rates and deposition of submarine fan complexes (e.g. Moki Formation).

During the late Miocene (10–8 Ma), the high sedimentation rate waned and an erosional unconformity is associated with approximately 250 m of missing section in the latest Miocene. The Pliocene was characterized by a return to high subsidence rates, high rates of sediment supply, and deposition of the thick shelfal to marginal marine Matemateaonga Formation. A period of uplift is modeled for the Quaternary, with the Cardiff-1 site experiencing c. 850 m of Pleistocene erosion.

Temperature profiles fit corrected bottom hole temperatures (Fig. 12) and reflect the variable burial rate, with modeled temperature based on measured well temperatures. Maximum temperatures were reached at c. 1.6 Ma at Cardiff-1, just prior to the onset of Pleistocene inversion. For base Mangahewa Formation, at a position equivalent to the K3EU reservoir, maximum temperatures are modeled at approximately 137°C. These temperatures are generally consistent with fluid-inclusion homogenization data measured from the edge of detrital grains or from overgrowth cements (Fig. 9). Some higher homogenization temperatures

(up to 165°C) have been measured, but most of these are from inclusions within the quartz grain (mid-grain) and are therefore presumed to be inherited temperatures from the sediment source (e.g., igneous source).

The 1D burial modeling suggests that at the Cardiff-1 site the late Cretaceous Rakopi Formation was mature for expelling oil from about 23 Ma to 6 Ma, and gas from about 11 Ma to the present day (Fig. 13). The base Paleocene and early-mid Eocene (Farewell and Kaimiro formations, respectively) are predicted to have been mature for oil expulsion since 8 Ma and 3 Ma, respectively, with the Farewell Formation mature for gas expulsion since c. 3 Ma (Fig. 13). The model suggests that the mid-late Eocene (Mangahewa Formation) has not yet reached sufficient maturity to expel oil or gas. This is supported by vitrinite reflectance data for the upper Mangahewa of 0.7% suggesting very early maturity for oil generation but not expulsion (Sykes 2001). Hence coaly source rocks within the Late Cretaceous to early-mid Eocene strata may have been expelling petroleum from c. 20 Ma to the present day, although rates of generation and consequent expulsion subsided through the uplift period. Notably, generation is not modeled to have ceased immediately upon uplift, but rather the thermal mass of the system is such that generation waned with cooling temperatures. It is likely that there have been several phases of expulsion and migration, with most of the early oil sourced from the older Rakopi Formation. Most of the gas expelled in the last 5 My is thought to have been generated from the same source, but with most of the oil expelled in the last 5 My sourced from the Paleocene–Eocene succession.

Multi-1D burial models developed at GNS Science (www.gns.cri.nz) suggest that kitchen areas lay to the east of Cardiff-1 and that these may have contributed to oil and gas accumulations in the Cardiff structure. Oil generation is thought to have been initiated as early as the Eocene in these areas, continuing to the mid-late Miocene. Gas generation started in the Oligocene–Miocene and continues to the present day (Stagpoole et al. 2004).

DISCUSSION

Synthesis of Diagenesis, Burial, and Fluid History

Petrology of samples from the K3E reservoir at Cardiff-1 show the sandstones to have undergone advanced diagenetic reactions, experiencing significant compaction and cementation by quartz and authigenic illite. In the following discussion, petrographic observations, fluid-inclusion microthermometry, and K-Ar dates are combined with the thermal model to illustrate relationships between the various diagenetic reactions, petroleum migration, and burial. This integrated approach elucidates the diagenetic and fluid-flow histories and has implications for both exploration and reservoir management of deep gas plays.

The relative timing of many diagenetic reactions was interpreted from paragenetic relationships observed in thin section. Early-formed authigenic minerals are relatively minor in the K3E reservoir sandstones at Cardiff-1 and are not discussed here in detail. They include products from eogenetic reactions and possible early carbonate cementation. Some clay transformations will also have taken place fairly early in the burial history, with the smectite–illite transformation possibly initiated as early as 30 Ma (50–75°C).

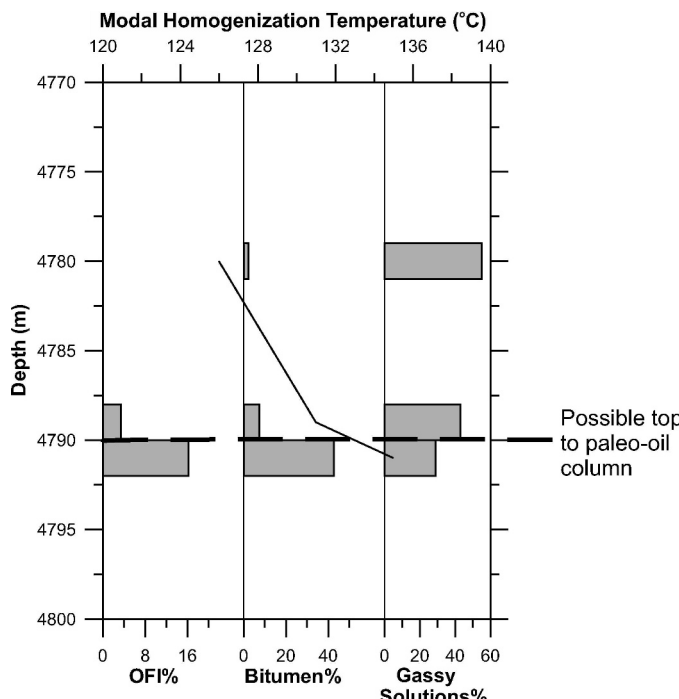


FIG. 10.—Relative abundances of quartz grains bearing oil inclusions (OFI%), bitumen and gassy saline solutions in Cardiff-1 and modal homogenization temperatures with depth.

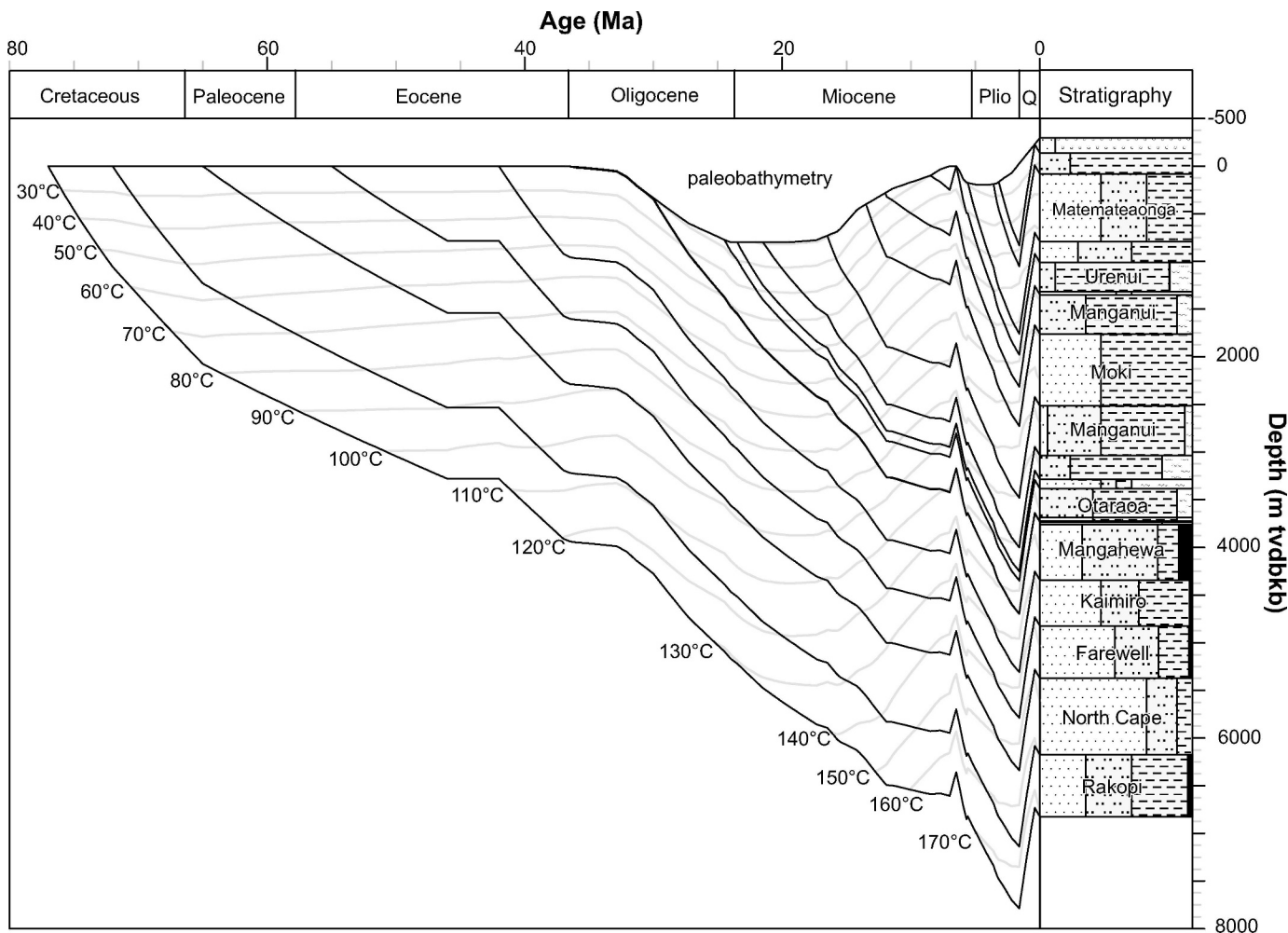


FIG. 11.—1-D burial and thermal history model for Cardiff-1 depicting incremental burial history (below sea level) for the Late Cretaceous through to the present. Isotherms are contoured downwards in 10°C increments from the 20°C isotherm. Paleobathymetry is indicated by the white polygon at the top of the chart. Horizons mapped below well TD (Farewell, North Cape, and Rakopi formations) are derived from isopach and structure maps.

Most diagenetic reactions that are thought to have significantly affected reservoir quality of the K3E reservoir have occurred in the last 15 million years, associated with fairly deep burial, temperatures in excess of 100°C, and oil and gas expulsion. Two stages of burial diagenesis are here proposed, the first involving reaction of feldspar to form authigenic kaolinite and quartz, and the second stage resulting in alteration of kaolinite to form illite. These reactions are discussed in the following section in relation to the burial, temperature, and fluid history, and are summarized in Figure 14.

(1) Stage 1.—It is suggested that much of the detrital feldspar in the reservoir underwent diagenetic reactions between c. 6 Ma and 13 Ma (c. 100–125°C; stage 1 in Fig. 14). At this time, reaction of feldspar was accompanied by precipitation of authigenic kaolinite and quartz and generation of some secondary porosity.

The most obvious source of acidity required to drive the feldspar reaction during burial diagenesis is through the generation of CO₂ as a result of the thermal degradation of kerogen during maturation (Schmidt and McDonald 1979; Surdam et al. 1984). Both the Cretaceous Rakopi Formation and the Paleocene–Eocene Kapuni Group in the Taranaki Basin contain locally significant coaly source rocks, and these locally thick, organic-rich, compacting and thermally maturing coaly

sequences could have provided important sources of acidic fluids affecting different regions in the basin at different times (Killops et al. 1996). This is supported by the presence of naturally occurring high CO₂ in gases derived from some Kapuni Group wells, onshore Taranaki, where the CO₂ has an isotopic composition consistent with thermogenic breakdown of organic matter in association with oil and condensate generation (Lyon 1989).

It is believed that the history of CO₂ expulsion at the Cardiff-1 site was extensive, with the Rakopi Formation expelling CO₂ from the mid-Eocene onwards (from c. 46 Ma), replaced by oil expulsion from c. 23 Ma. However, given the thick stratigraphic section, any acidic fluids derived at the Cardiff site from deep Cretaceous source rocks are likely to have been neutralized by the time they reached the K3E reservoir. It is considered here that dissolution within the K3E is more likely to have occurred by CO₂ generated from intraformational coaly source rocks (Fig. 14). The Paleocene Kapuni Group is modeled to have started CO₂ expulsion in the early Miocene (from c. 18 Ma), with the mid-late Eocene mature for CO₂ expulsion by the end of the Miocene (from c. 10 Ma). This modeled CO₂ expulsion from the Kapuni Group is consistent with homogenization temperatures from aqueous inclusions within quartz overgrowths or dust rims, suggesting trapping temperatures of $\geq 100^\circ\text{C}$ (assuming no pressure corrections; Fig. 14), corresponding to c. 8–12 Ma.

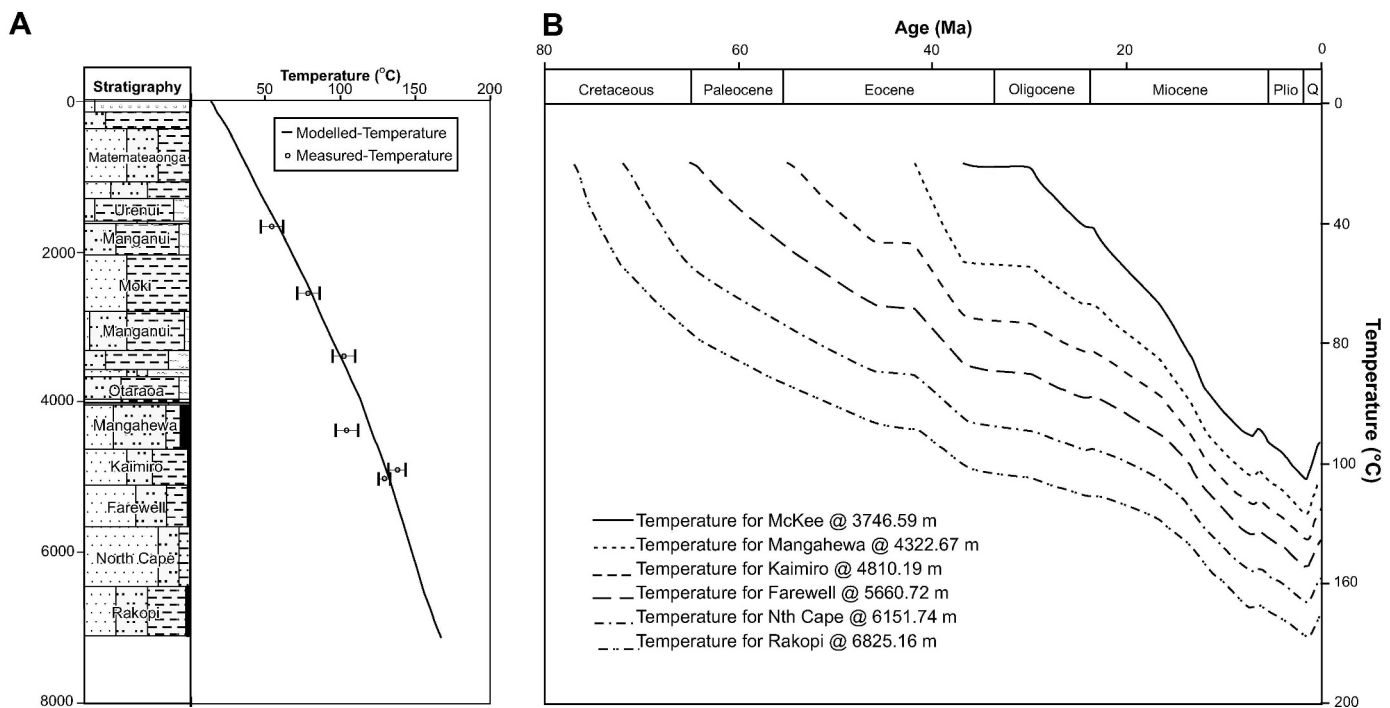


FIG. 12.—A) Predicted temperature–depth curve with corrected bottom-hole temperatures depicted as circles with error bars. B) Temperature-history model for Cardiff-1, with tracked horizons in ascending order: Rakopi, North Cape, Farewell, Kaimiro, and Mangahewa formations.

It therefore seems likely that the stage 1 reaction was driven by circulation of CO₂-rich fluids generated by thermogenic maturation of Paleocene–Eocene coaly source rocks.

The Cretaceous Rakopi Formation, which is the main source rock in the Taranaki Basin, was mature for oil expulsion at the same time in the burial history that the Paleogene source rocks were mature for CO₂ expulsion (Fig. 14). There is considerable evidence in the K3E sandstones that oil has migrated into the reservoir, whilst the presence of residual oil lining secondary pores suggests that petroleum migration occurred after feldspar dissolution had started. There were probably several phases of oil charging, but these are difficult to distinguish because of the unknown fluid compositions. Interpretation of homogenization temperatures from oil-filled inclusions is complicated by gas content, and without information on fluid composition (and the necessary corrections) Th must be thought of as minimum trapping temperatures. Using these assumptions, data from oil fluid inclusions supports charging of the main phase of oil in the mid-Miocene between 10 and 8 Ma (115 and 120°C minimum temperatures), after development of the structural trap (earliest Miocene; STOS 1992). In addition, homogenization temperatures for aqueous inclusions associated with oil-filled inclusions indicate that oil was present in the reservoir at c. 117°C (assuming no pressure corrections), corresponding to c. 10 Ma, a time when the Rakopi Formation was mature for oil expulsion (Fig. 14).

In summary, the main stage 1 reactions occurred during burial diagenesis in the mid-late Miocene (c. 7–13 Ma). It is possible that some CO₂-rich fluids and oil may have passed through the reservoir at a much earlier stage, associated with maturation of the Rakopi source in adjacent kitchen areas (mature for oil expulsion from the Eocene). However, the mid-Miocene interpolated for paleo-oil saturated porefluids is more likely associated with fluids derived from a local source. The end of this stage of diagenesis is therefore tentatively taken at c. 6 Ma, the approximate time for the end of oil expulsion from the Rakopi Formation. This timing is consistent with a homogenization temperature of 125°C measured from aqueous inclusions associated with hydrocarbon-bearing inclusions with daughter minerals.

(2) Stage 2.—The second stage of burial diagenesis is proposed to have occurred between c. 5 Ma to the present day and is dominated by the reaction of kaolinite to form illite and quartz. This is suggested by petrographic evidence for transformations of much of the earlier-formed kaolinite to illite during late diagenesis. The presence of illite as opposed to dickite, the high-temperature and high-pressure polymorph of kaolinite, requires a source of potassium in the porefluids, which is most likely to have come from reactions with K-feldspar.

The timing for illitization comes from K-Ar dating of authigenic illites, which dates the illite (< 2 µm fraction) at c. 4.5 Ma. This equates to a time of tectonism when regional uplift and inversion of previous structures was widespread in the Taranaki Basin (Browne 2004; King 2000; Nelson and Hume 1977). Microthermometry of aqueous inclusions associated with quartz overgrowths demonstrates a range of Th from c. 100°C to 135°C, with the main peak at 130–135°C. This could be evidence for a second phase of quartz cementation occurring very late in diagenesis and associated with illitization (Fig. 14); some secondary quartz was probably also derived from late-stage chemical compaction. These data are consistent with paragenetic relationships which show late-stage quartz cements postdating oil emplacement (quartz cement enclosing residual oil).

The K3E reservoir at Cardiff-1 is currently gas charged, and therefore it is assumed that oil was displaced by gas during late-stage burial. This is supported by the gassy nature of fluid inclusions at Cardiff-1. A late phase of expulsion corresponding to c. 3–0 Ma is envisaged, which would be consistent with high homogenization temperatures measured from gassy aqueous fluid inclusions associated with Type 3 gas inclusions (Th = 135°C).

Despite intense illitization, some large secondary pores, commonly lined with residual oil, have been preserved in the K3E reservoir. It is therefore likely that authigenic illite formed prior to displacement of the oil and possibly within oil-saturated porefluids. There has been significant debate recently about the effect of hydrocarbon emplacement on cementation (e.g., Walderhaug 1994; Bloch et al. 2002). Some authors have suggested that oil may retard but not necessarily halt cementation (e.g., Worden et al.

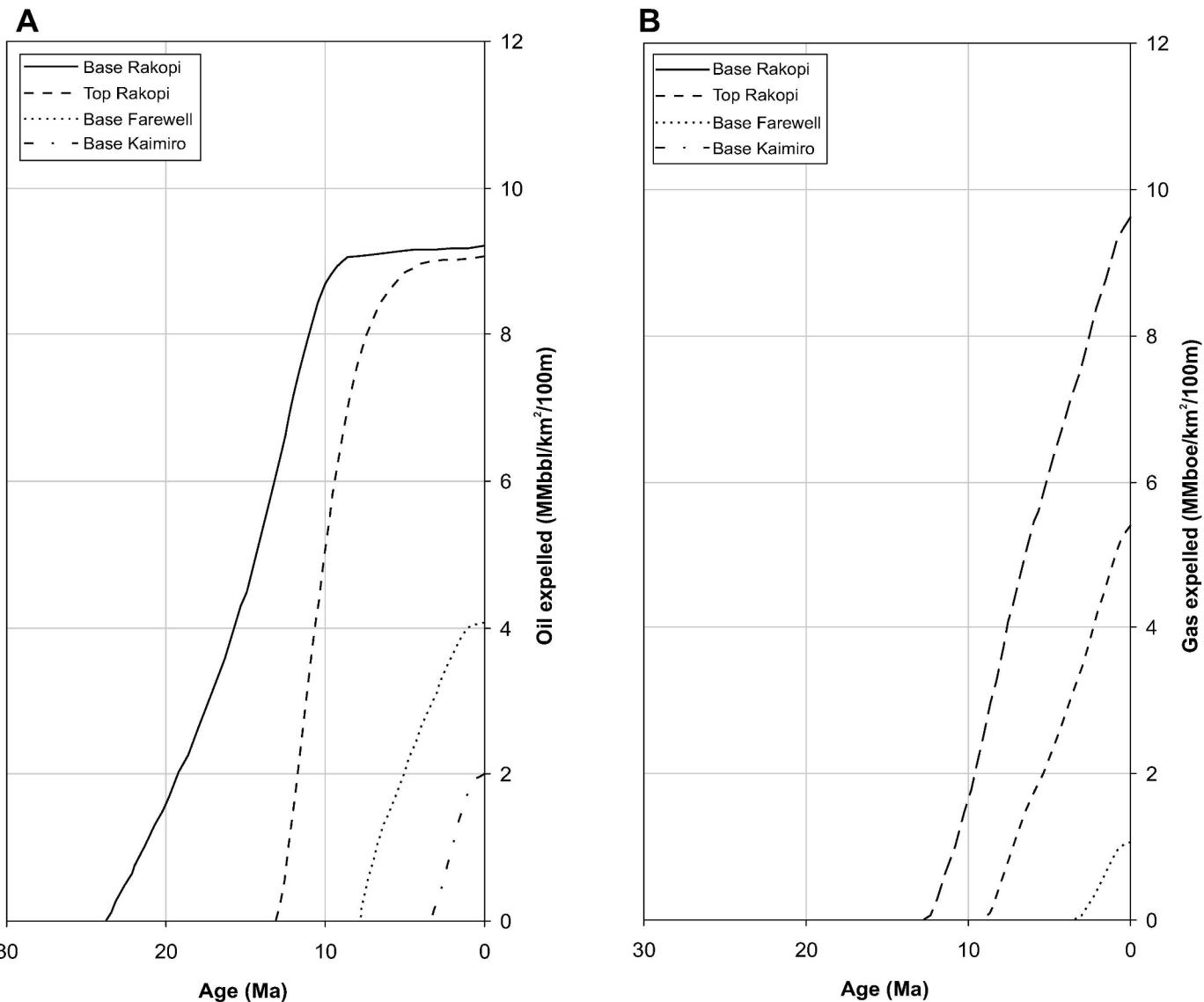


FIG. 13.—Volumes of A) oil and B) gas expelled through time for the main source rocks at Cardiff-1; the Mangahewa Formation did not reach maturities for expulsion. Predicted volumes (in MMbbl oil and MM barrel oil equivalent gas) are given for a square-kilometer area and 100 m-thick source-rock unit assuming source-rock parameters as quoted in the text.

1998). Ehrenberg and Nadeau (1989) have suggested that 20–30% residual water saturation is sufficient for extensive illitization to occur by short-range diffusive transport in a compositionally closed system, whilst Thyne et al. (2001) have shown in simulations of the Statfjord Formation of the North Sea that oil emplacement did not stop illitization but did limit potassium mobility and maximized illite formation within the sandstone. All of the results from these published papers are supportive of the proposed sequence observed in Cardiff-1 (Fig. 14).

The change in the nature of the petroleum charge reflects the changing gas:oil ratio of the system as the maturing source rocks supply increasing quantities of gas. At the Cardiff-1 wellsite, the primary source of gas was from the upper Cretaceous Rakopi Formation during the early to late Miocene, with gas production continuing to the present day (16 Ma to the present day). A secondary source of gas may have been derived from the Paleocene and early Eocene source rocks from the late Miocene to the present day (Fig. 13).

Implications for Reservoir Quality

Low permeabilities have been reported from the K3E reservoir at Cardiff-1 despite fair to moderate measured porosity values. Scatter plots of IGV and authigenic minerals versus permeability are evidence that significant compaction (low IGV) and abundant quartz cements and authigenic illites are controlling the present-day variation in permeability (Fig. 15) and are therefore responsible for the poor reservoir quality observed at Cardiff-1.

Mechanical and chemical compaction has played an important part in reducing depositional porosities to their present values, with chemical compaction probably sourcing some silica for precipitation as quartz overgrowth cements. These cements (also sourced by reactions with feldspar grains) have occluded some IGV, resulting in further porosity loss. Whilst compaction and quartz cementation have reduced pore volumes, the precipitation of authigenic illite is interpreted as a major control on permeability.

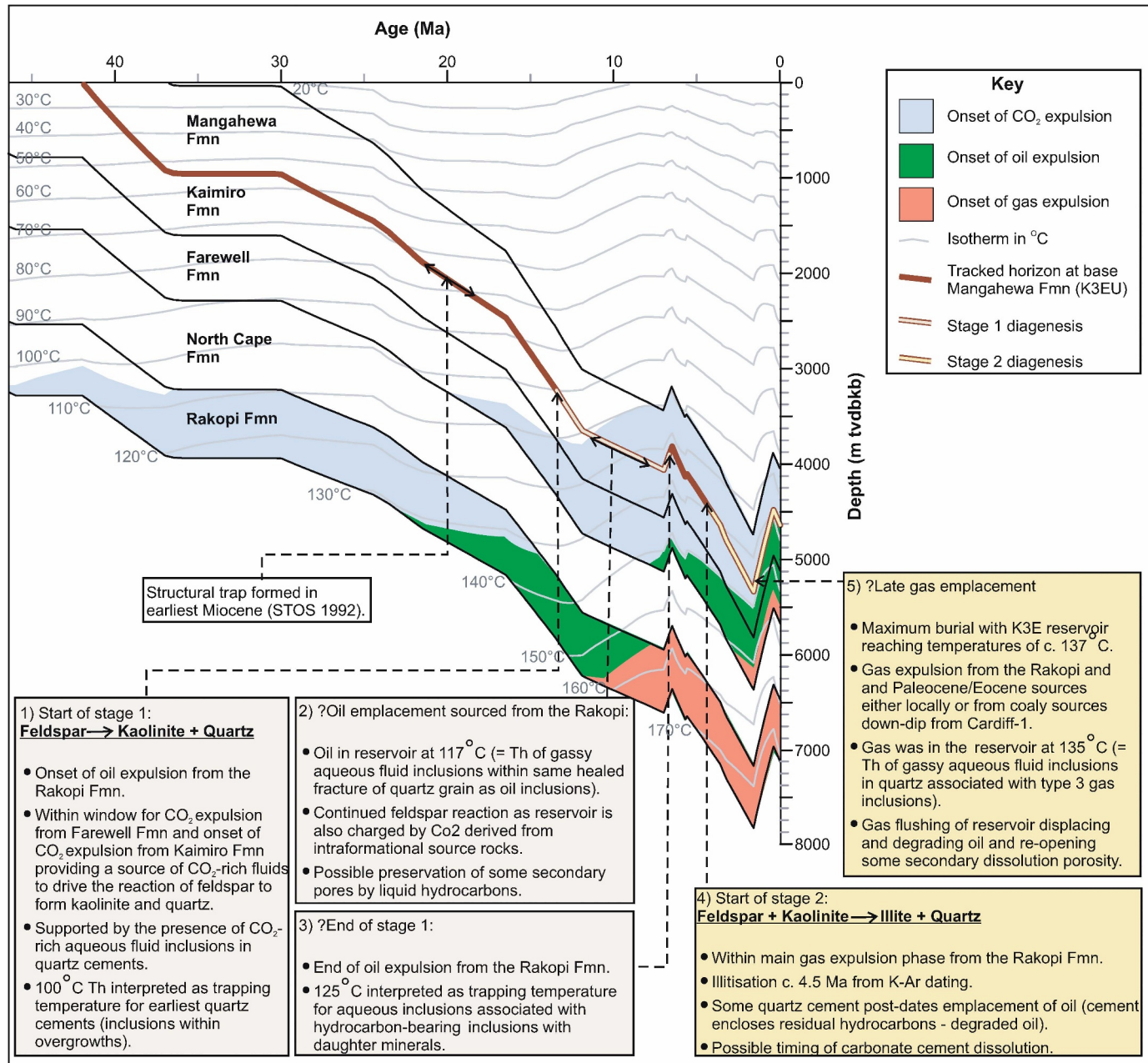


FIG. 14.—Summary of the main diagenetic reactions relative to the burial and charge history.

Illite is known to have a severe detrimental effect on reservoir quality (e.g., Thyne et al. 2001) by reducing pore size and increasing pore tortuosity.

Secondary-dissolution pores are the main type of macropore in the Cardiff-1 samples. However, despite the evidence suggesting that a significant amount of feldspar has undergone reaction, there has been only minor generation of secondary macroporosity, and instead most feldspars are replaced by clay minerals. The rare, locally large secondary pores may have been preserved through occlusion by oil (thus locally preventing illite from forming).

Cementation, illitization, and associated destruction of reservoir quality occurred very late in the diagenetic history at Cardiff-1. Timing is thought to be related to a late-stage reaction, possibly associated with gas-matured sources. It is suggested that better reservoir performance can be expected only where extensive illitization has not occurred, i.e., where

there is no source of potassium or where temperatures are lower than c. 120–130 $^{\circ}\text{C}$ (and therefore where kaolinite will form in preference to illite). Potassium, however, is still available in the K3E reservoir sandstone today in the form of minor remnant K-feldspar. Regarding temperatures, both the 1-D basin model presented here and in-house data from GNS Science (www.gns.cri.nz) show that the K3EU reservoir at Cardiff-1 reached temperatures of > 120 $^{\circ}\text{C}$ by the late Miocene and therefore temperatures of < 120 $^{\circ}\text{C}$ are unlikely in the nearby vicinity. These factors imply significant risk associated with predicting good reservoir performance in the mid-late Eocene reservoirs at Cardiff.

Implications for the Petroleum Industry

Despite poor reservoir quality of the K3E sandstones at Cardiff-1, the presence of a gas column and 1–5% observed large, illite-free secondary

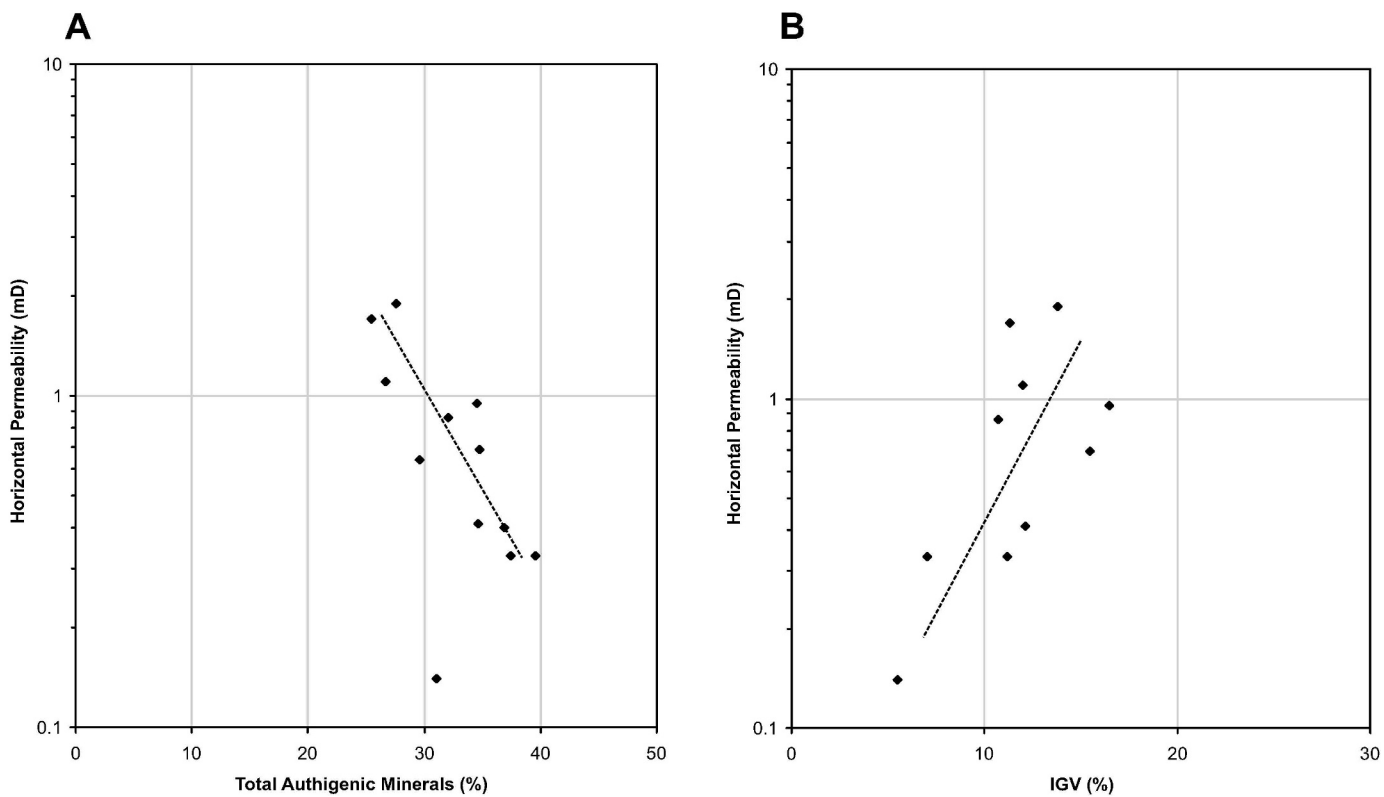


FIG. 15.—Scatter plot of petrographic data showing controls on permeability. A) Overall negative correlation between total authigenic minerals (predominantly quartz cement and illite) and permeability. B) Overall positive correlation between intergranular volume (IGV) and permeability.

pores is reason to retain the Cardiff structure as a potential deep (Eocene) gas play. Gas production is more likely to be commercially viable today compared to the early 1990s due to the currently buoyant gas market and improved production techniques (e.g., hydraulic fracturing). In addition, the results from this study suggest that gas in the reservoir has displaced an earlier oil phase. This provides a new exploration play with the possibility for redistribution of oil into an adjacent up-dip trap.

Whilst this study was undertaken entirely independently of the petroleum industry, at the time of writing, evaluation of potential plays in the Cardiff area was underway by a New Zealand company (Austral Pacific Energy, Ltd.). Good gas shows were encountered in the mid-late Eocene sandstones at Cardiff-2A/2B, and oil was discovered within shallower Miocene reservoirs at Cheal, a structure located c. 3 km to the SE of Cardiff-1. It is unknown whether either Cardiff or Cheal will produce commercial quantities of petroleum, and indeed whether the oil in Miocene reservoirs at Cheal represents redistributed oil from Cardiff. However, the results from this study demonstrate the value of interrogating existing data using multidisciplinary techniques. This approach could be applied to other bypassed gas shows both in New Zealand and overseas.

CONCLUSIONS

- Poor reservoir quality in the mid-Eocene sandstones at Cardiff-1 is due to a combination of compactional effects (mechanical and chemical), quartz cementation, and illitization.
- The sandstones are interpreted to have been moderately feldspar-rich on deposition, with petrographic results consistent with c. 21% of feldspar having undergone reaction during burial diagenesis to form microporous authigenic kaolinite, quartz cements, and minor secondary porosity.

- The feldspar reaction is thought to have been driven by circulation of CO₂-rich fluids generated by thermogenic maturation of Paleocene–Eocene coaly source rocks between c. 7 Ma and 13 Ma (c. 100–125°C).
- Petrographic and fluid-inclusion evidence suggests that oil migrated into the reservoir after some kaolinite precipitation.
- Diagenetic illites, which have had a detrimental effect on reservoir quality in mid-late Eocene sandstones at Cardiff-1, are interpreted to have formed by transformation from kaolinite within the last 5 Ma at temperatures of c. 130–135°C.
- Petrographic observations and fluid-inclusion data suggest that a second phase of quartz cementation also occurred very late in diagenesis, within the last 5 Ma and close to maximum burial temperatures.
- Some large and illite-free pores are observed in the sandstones; these pores may have been preserved by oil, with subsequent displacement of the oil by gas. Macroporosity currently constitutes approximately 15–45% of the total porosity, with the remainder occurring as micropores.
- A late gas charge (c. 3 Ma to present day) sourced either locally or from coaly source rocks down-dip from Cardiff-1 is consistent with high homogenization temperatures measured from inclusions in quartz cements.
- Given the currently buoyant gas market, together with advances in modern production techniques (e.g., hydraulic fracturing), it may now be economic to flow gas from the locally large, but isolated, pores identified in the K3E reservoir. In addition, the potential for redistributed petroleum into up-dip traps represents a new exploration play.

ACKNOWLEDGMENTS

This project has been part funded by the Foundation for Research, Science and Technology under contract No. CO5X0302. The authors would like to thank Neville Orr for preparation of thin sections and Ray Soong for XRD analysis. Brad Field, Vaughan Stagpoole, Greg Browne, Malcolm Arnot, Richard Worden, Calum Macauley, Sasha Haddad and Robert Pottorf are thanked for their helpful comments on the manuscript. We acknowledge the use of Genesis modeling software from Zetaware, Inc.

REFERENCES

- ARMSTRONG, P.A., AND CHAPMAN, D.S., 1999, Combining tectonic and temperature evolution in Taranaki Basin, *in* Forster, A., and Merriam, D., eds., *Geothermics in Basin Analysis*: Dordrecht, The Netherlands, Kluwer/Plenum, p. 151–176.
- BEARD, D.C., AND WEYL, P.K., 1973, Influence of texture on porosity and permeability of unconsolidated sand: American Association of Petroleum Geologists, Bulletin, v. 57, p. 349–369.
- BØRLYKKE, K., 1984, Formation of secondary porosity: how important is it? *in* Surdam, R.C., and McDonald, D.A., eds., *Clastic Diagenesis*: American Association of Petroleum Geologists, Memoir 37, p. 277–286.
- BLOCH, S., AND FRANKS, S.G., 1993, Preservation of shallow plagioclase dissolution porosity during burial: implications for porosity prediction and aluminium mass balance: American Association of Petroleum Geologists, Bulletin, v. 77, p. 1488–1501.
- BLOCH, S., LANDER, R.H., AND BONNEAU, L., 2002, Anomalously high porosity and permeability in deeply buried sandstone reservoirs: origin and predictability: American Association of Petroleum Geologists, Bulletin, v. 86, p. 301–328.
- BONHOMME, M.G., THUIZAT, R., PINAULT, Y., CLAUER, N., WENDLING, R., AND WINKLER, R., 1975, Méthode de datation potassium-argon: appareillage et technique: Strasbourg, Note Technique, l’Institut de Géologie, n. 3, 53 p.
- BROWNE, G.H., 2004, Late Neogene sedimentation adjacent to the tectonically evolving North axial ranges: insights from Kuripapango, western Hawke’s Bay: New Zealand Journal of Geology and Geophysics, v. 47, p. 663–674.
- BRYANT, I.D., AND BARTLETT, A.D., 1991, Kapuni 3D reservoir model and reservoir simulation: Proceedings of the 1991 New Zealand Oil Exploration Conference, Ministry of Commerce, p. 404–412.
- BURCIK, E.J., 1979, Properties of petroleum reservoir fluids: Boston, U.S.A., IHRDC, 190 p.
- BURNHAM, A.K., AND SWEENEY, J.J., 1989, A chemical kinetic model of vitrinite maturation and reflectance: *Geochimica et Cosmochimica Acta*, v. 53, p. 2649–2657.
- CORE LABORATORIES, 1992, Core analysis report, Cardiff-1, *in* STOS, 1992, Well resume—Cardiff-1 PPL 38707 onshore Taranaki Basin, New Zealand, unpublished New Zealand petroleum report 1844.
- EHRENBERG, S.N., AND NADEAU, P.H., 1989, Formation of diagenetic illite in sandstones of the Garn Formation, Haltenbanken area, Mid-Norwegian continental shelf: Clay Minerals, v. 24, p. 233–253.
- FOLK, R.L., ANDREWS, P.B., AND LEWIS, D.W., 1970, Detrital sedimentary rock classification and nomenclature for use in New Zealand: New Zealand Journal of Geology and Geophysics, v. 13, p. 937–968.
- FUNNELL, R.H., CHAPMAN, D.S., ALLIS, R.G., AND ARMSTRONG, P.A., 1996, Thermal state of the Taranaki Basin, New Zealand: Journal of Geophysical Research, v. 101, p. 25197–25215.
- Geotechnical Services, 1992, Petrology on core 2 samples, Cardiff-1, *in* STOS, 1992, Well resume—Cardiff-1 PPL 38707 onshore Taranaki Basin, New Zealand, unpublished New Zealand petroleum report 1844.
- HAMILTON, P.J., GILES, M.R., AND AINSWORTH, P., 1992, K-Ar dating of illites in Brent Group reservoirs: a regional perspective, *in* Morton, A.C., Haszeldine, R.S., Giles, M.R., and Brown, S., eds., *Geology of the Brent Group*: Geological Society of London, Special Publication 61, p. 377–400.
- HANOR, J.S., 1980, Dissolved methane in sedimentary brines: potential effect on the PVT properties of fluid inclusions: Economic Geology, v. 75, p. 603–617.
- HEDENQUIST, J.W., AND HENLEY, R.W., 1985, Effect of CO_2 on freezing point depression measurements of fluid inclusions: evidence from active geothermal systems and implications for epithermal ore deposits: Economic Geology, v. 80, p. 1379–1406.
- HEINRICHS, H., AND HERRMANN, A.G., 1990, *Praktikum der Analytischen Geochemie; Practical Handbook for Analytical Geochemistry*: Berlin, Springer-Verlag, 669 p.
- HOUSEKNIGHT, D.W., 1987, Assessing the relative importance of compaction processes and cementation to reduction of porosity in sandstones: American Association of Petroleum Geologists, Bulletin, v. 71, p. 633–642.
- KILLOPS, S.D., ALLIS, R.G., AND FUNNELL, R.H., 1996, Carbon dioxide generation from coals in Taranaki Basin, New Zealand: implications for petroleum migration in southeast Asian Tertiary basins: American Association of Petroleum Geologists, Bulletin, v. 80, p. 545–569.
- KING, P.R., 2000, Tectonic reconstructions of New Zealand: 40 Ma to the Present: New Zealand Journal of Geology and Geophysics, v. 43, p. 611–638.
- KING, P.R., AND THRASHER, G.P., 1996, Cretaceous-Cenozoic geology and petroleum systems of the Taranaki Basin, New Zealand: Institute of Geological and Nuclear Sciences, Monograph 13, 244 p.
- LAND, L.S., 1984, Frio Sandstone diagenesis, Texas Gulf Coast: a regional isotopic study, *in* Surdam, R.C., and McDonald, D.A., eds., *Clastic Diagenesis*: American Association of Petroleum Geologists, Memoir 37, p. 47–62.
- LANDER, R.H., AND WALDERHAUG, O., 1999, Predicting porosity through simulating sandstone compaction and quartz cementation: American Association of Petroleum Geologists, Bulletin, v. 83, p. 433–449.
- LEE, M., ARONSON, J.L., AND SAVIN, S.M., 1985, K/Ar dating of Rotliegendes sandstone, Netherlands: American Association of Petroleum Geologists, Bulletin, v. 69, p. 1381–1385.
- LIEWIG, N., CLAUER, N., AND SOMMER, F., 1987, Rb-Sr and K-Ar dating of clay diagenesis in Jurassic sandstone oil reservoirs, North Sea: American Association of Petroleum Geologists, Bulletin, v. 71, p. 1467–1474.
- LISK, M., BRINCAT, M.P., EADINGTON, P.J., AND O’BRIEN, G.W., 1998, Hydrocarbon charge in the Vulcan sub-basin, *in* Purcell, P.G., and Purcell, R.R., eds., *The Sedimentary Basins of Western Australia 2: Proceedings of the West Australian Basins Symposium*, p. 287–305.
- LYON, G.L., 1989, The stable isotope composition of some North Island natural gases: Report RD8807, Ministry of Energy, Wellington, 26 p.
- MCDOUGALL, I., AND ROKSANDIC, Z., 1974, Total fusion $^{40}\text{Ar}/^{39}\text{Ar}$ ages using HIFAR reactor: Geological Society of Australia, Journal, v. 21, p. 81–89.
- MEUNIER, A., AND VELDE, B., 2004, *Illite: Origins, Evolution and Metamorphism*: Berlin, Springer, 286 p.
- NELSON, C.S., AND HUME, T.M., 1977, Relative intensity of tectonic events revealed by the Tertiary sedimentary record in the North Wanganui Basin and adjacent areas: New Zealand: New Zealand Journal of Geology and Geophysics, v. 20, p. 369–392.
- PEPPER, A.S., AND CORVI, P.J., 1995a, Simple kinetic models of petroleum formation. Part 1: oil and gas generation from kerogen: Marine and Petroleum Geology, v. 12, p. 291–319.
- PEPPER, A.S., AND CORVI, P.J., 1995b, Simple kinetic models of petroleum formation. Part III: modelling an open system: Marine and Petroleum Geology, v. 12, p. 417–452.
- PEVEAR, D.R., 1999, Illite and hydrocarbon exploration: National Academy of Science (U.S.A.) Proceedings, v. 96, p. 3440–3446.
- RAMM, M., AND BØRLYKKE, K., 1994, Porosity/depth trends in reservoir sandstones: assessing the quantitative effects of varying pore-pressure, temperature history and mineralogy, Norwegian Shelf data: Clay Minerals, v. 29, p. 475–490.
- ROEDDER, E., 1984, Fluid inclusions: Washington, Mineralogical Society of America: Reviews in Mineralogy, v. 12, 644 p.
- SCHMIDT, V., AND McDONALD, D.A., 1979, The role of secondary porosity in the course of sandstone diagenesis, *in* Scholle, P.A., and Schlager, P.R., eds., *Aspects of Diagenesis*: Society of Economic Paleontologists and Mineralogists, Special Publication 26, p. 175–207.
- SIEBERT, R.M., MONCURE, G.K., AND LAHANN, R.W., 1984, A theory of grain dissolution in sandstones, *in* Surdam, R.C., and McDonald, D.A., eds., *Clastic Diagenesis*: American Association of Petroleum Geologists, Memoir 37, p. 163–175.
- SMALE, D., 1996, Petrographic summaries of Taranaki petroleum reports: New Zealand, Institute of Geological and Nuclear Sciences, Science Report 96/1, 88 p.
- STAGPOOLE, V., FUNNELL, R., AND NICOL, A., 2004, Overview of the structure and associated petroleum prospectivity of the Taranaki Fault, New Zealand: The Petroleum Exploration Society of Australia, Eastern Australian Basins Symposium II, p. 197–206.
- STEIGER, R.H., AND JÄGER, E., 1977, Subcommission on Geochronology: convention on the use of decay constants in geo- and cosmochronology: Earth and Planetary Science Letters, v. 36, p. 359–362.
- STORVOLL, V., BØRLYKKE, K., KARLSEN, D., AND SAIGAL, G., 2002, Porosity preservation in reservoir sandstones due to grain-coating illite: a study of the Jurassic Garn Formation from the Kristin and Lavrans fields, offshore Mid-Norway: Marine and Petroleum Geology, v. 19, p. 767–781.
- STOS, 1992, Well resume—Cardiff-1 PPL 38707 onshore Taranaki Basin, New Zealand: unpublished New Zealand petroleum report 1844.
- SURDAM, R.C., BOESE, S.W., AND CROSSEY, L.J., 1984, The chemistry of secondary porosity, *in* Surdam, R.C., and McDonald, D.A., eds., *Clastic Diagenesis*: American Association of Petroleum Geologists, Memoir 37, p. 127–150.
- SYKES, R., 2001, Depositional and rank controls on the petroleum potential of coaly source rocks: The Petroleum Exploration Society of Australia, Eastern Australian Basins Symposium, p. 591–602.
- THRASHER, G.P., AND CAHILL, J.P., 1990, Subsurface maps of the Taranaki Basin region, New Zealand: New Zealand Geological Survey, Report G 142, 45 p. 14 sheets.
- THYNE, G., BOUDREAU, B.P., RAMM, M., AND MIDTBØ, R.E., 2001, Simulation of potassium feldspar dissolution in the Statfjord Formation, North Sea: American Association of Petroleum Geologists, Bulletin, v. 85, p. 621–635.
- TSENG, H.Y., AND POTTORF, R.J., 2002, Fluid inclusion constraints on petroleum PVT and compositional history of the Greater Alwyn–South Brent petroleum system, southern North Sea: Marine and Petroleum Geology, v. 19, p. 797–809.
- WALDERHAUG, O., 1994, Precipitation rates of quartz cement in sandstones determined by fluid-inclusion microthermometry and temperature-history modelling: Journal of Sedimentary Research, v. 64, p. 324–333.
- WALDERHAUG, O., 2000, Modeling quartz cementation and porosity in Middle Jurassic Brent Group sandstones of the Kvitebjørn Field, Northern North Sea: American Association of Petroleum Geologists, Bulletin, v. 84, p. 1325–1339.
- WORDEN, R.H., OXTOBY, N.H., AND SMALLEY, P.C., 1998, Can oil emplacement prevent quartz cementation in sandstones?: Petroleum Geoscience, v. 4, p. 129–137.